

Mixed Modes and Asteroseismic Surface Effects: I. Analytic TreatmentJ. M. JOEL ONG (王加冕) ¹, SARBANI BASU ¹ AND IAN W. ROXBURGH ²¹*Department of Astronomy, Yale University, 52 Hillhouse Ave., New Haven, CT 06511, USA*²*Astronomy Unit, Queen Mary University of London, Mile End Road, London E1 4NS, UK*

(Received June 4, 2021; Revised July 5, 2021; Accepted July 6, 2021)

ABSTRACT

Normal-mode oscillation frequencies computed from stellar models differ from those which would be measured from stars with identical interior structures, because of modelling errors in the near-surface layers. These frequency differences are referred to as the asteroseismic "surface term". The vast majority of solar-like oscillators which have been observed, and which are expected to be observed in the near future, are evolved stars which exhibit mixed modes. For these evolved stars, the inference of stellar properties from these mode frequencies has been shown to depend on how this surface term is corrected for. We show that existing parametrisations of the surface term account for mode mixing only to first order in perturbation theory, if at all, and therefore may not be adequate for evolved stars. Moreover, existing nonparametric treatments of the surface term do not account for mode mixing. We derive both a first-order construction, and a more general approach, for one particular class of nonparametric methods. We illustrate the limits of first-order approximations from both analytic considerations and using numerical injection-recovery tests on stellar models. First-order corrections for the surface term are strictly only applicable where the size of the surface term is much smaller than both the coupling strength between the mixed p- and g-modes, as well as the local g-mode spacing. Our more general matrix construction may be applied to evolved stars, where perturbation theory cannot be relied upon.

Unified Astronomy Thesaurus Concepts: Asteroseismology (73), Stellar oscillations (1617), Computational methods (1965), Theoretical techniques (2093)

1. INTRODUCTION AND MOTIVATION

High-cadence stellar photometry from space missions like *CoRoT*, *Kepler*, and *TESS* (and soon *CHEOPS*, *PLATO*, and others) has enabled the detection of solar-like oscillations in stars spanning a broad range of evolutionary stages and masses, as well as the measurement of their oscillation frequencies with high precision. However, efforts to use these measurements to constrain the properties of these stars, as was done to great effect for the Sun with helioseismology, are fundamentally limited by deficiencies in modelling their surface layers. As a result of these modelling errors, the normal-mode oscillation frequencies computed from stellar models necessarily differ from those which would be measured from stars with identical global properties and interior structures. These frequency differences are collectively referred to as the asteroseismic "surface term". For p-modes, the surface term

is understood to be a slowly varying function of frequency, whose magnitude also increases with frequency.

Ong et al. (2021) showed that the behaviour of the surface term exhibits qualitative differences between main-sequence stars and more evolved (red giant) stars. In particular, they confirmed (following Basu & Kinnane 2018) that parametric methods like the proposed correction of Ball & Gizon (2014, hereafter *BG14*) yield estimates of the stellar mass, radius, and age which are comparable to those returned by nonparametric methods, such as separation ratios (Roxburgh & Vorontsov 2003; Oti Floranes et al. 2005; Roxburgh 2005) and phase offsets (Roxburgh 2016), when applied to stars on the main sequence. However, they also demonstrated that the use of these two nonparametric methods yielded ensemble estimates of these same properties that differed from those obtained using the *BG14* correction, when applied to red giants in the open cluster NGC 6791. Since many other parametric corrections — motivated either by solar observations (Kjeldsen et al. 2008), or from MHD simulations (Sonoii et al. 2015) — all yield estimates of these properties which are similar to the *BG14* correction on this open cluster (Jørgensen et al.

2020), this was suggestive of a qualitative difference between parametric and nonparametric treatments of the surface term in these evolved oscillators. Furthermore, this leaves open the possibility of some hitherto unexplored transition between main-sequence-like and red-giant-like surface terms, as reflected by how the results of parametric and nonparametric treatments differ.

Ideally, we should investigate such a transition by examining potential differences between both classes of surface-term treatments when applied to stars in intermediate evolutionary phases (subgiants), since this might be instructive as to when, or how, this qualitative change occurs (or if there is a sharp transition at all). However, the oscillation frequencies of subgiant stars exhibit significant, qualitative differences from those of both main-sequence stars and more evolved red giants. In particular, evolved solar-like oscillators support both acoustic p -waves (in the convective exterior), and buoyancy g -waves (in the radiative interior). Mathematically, these are described by two independent sets of π and γ modes (in the sense of Aizenman et al. 1977; Ong & Basu 2020), whose mode cavities are coupled to each other evanescently. The normal-mode frequencies which we measure are not these “bare” π and γ mode frequencies, but have been “screened,” both by self-interaction (to yield p and g -modes), and by coupling to each other to yield mixed modes.

In the two regimes which we have previously examined, we have observational access to either pure p -modes (for main sequence stars) or close to pure π -modes (for red giants). On the other hand, subgiant stars, which lie between these two regimes, exhibit isolated avoided crossings with very strong coupling between the π and γ mode cavities, so that the quantities which are used in nonparametric treatments of the surface term cannot easily be estimated from their measured frequency sets. Consequently, these methods cannot be directly applied to such subgiants. Likewise, the extent to which existing parametrisations of the surface term, including that of BG14, remain valid in the presence of mode mixing is still largely unexplored.

In this paper, we provide constructions generalising those of BG14 and of Roxburgh (2016), exploiting recent theoretical developments (Ong & Basu 2020, hereafter OB20) permitting the evaluation of the bare π - and γ -mode eigensystem of a stellar model, as well as of their corresponding coupling matrices in closed form. Using this, we examine the limits of validity of existing approaches to the surface term in the presence of mode mixing (Section 2). We also extend one class of nonparametric treatments of the surface term (the ϵ -matching algorithm of Roxburgh 2016) to explicitly take mode coupling into account, and examine various sources of systematic error committed in our construction (Section 3). We then demonstrate the utility of these generalisations in modelling stars exhibiting such isolated avoided crossings, by employing these procedures in an injection-recovery test on stellar models, and assess the practical significance of this systematic error (Section 4). In the companion paper to this

work (Ong et al. submitted to ApJ, hereafter Paper II), we use the procedures outlined here to investigate the behaviour of the surface term, characterised through these constructions, as seen in a larger sample of various subgiants observed by the *Kepler* and K2 missions.

2. PERTURBATION ANALYSIS

The avoided crossings with which we are concerned arise owing to the coupling of two otherwise disjoint acoustic systems, whose frequencies are close to resonance. In general, these frequencies are the eigenvalues of some time-independent wave operator $\hat{\mathcal{L}}$ associated with the stellar structure. OB20 described a decomposition of this wave operator into separate π and γ wave operators $\hat{\mathcal{L}}_\pi, \hat{\mathcal{L}}_\gamma$ — constructed so as to suppress wave propagation of the each type separately — and their remainder operators $\hat{\mathcal{R}}_\pi, \hat{\mathcal{R}}_\gamma$. Having done so, they then derived analytic expressions for the matrix elements of a generalised Hermitian eigenvalue problem (GHEP) of the form

$$\begin{aligned} \begin{bmatrix} \mathbf{L}_\pi & \mathbf{L}_{\pi\gamma} \\ \mathbf{L}_{\pi\gamma}^\dagger & \mathbf{L}_\gamma \end{bmatrix} \mathbf{c}_i &= \begin{bmatrix} -\Omega_\pi^2 + \mathbf{R}_{\pi\pi} & -\Omega_\pi^2 \mathbf{D}_{\pi\gamma} + \mathbf{R}_{\pi\gamma} \\ \left(-\Omega_\pi^2 \mathbf{D}_{\pi\gamma} + \mathbf{R}_{\pi\gamma}\right)^\dagger & -\Omega_\gamma^2 + \mathbf{R}_{\gamma\gamma} \end{bmatrix} \mathbf{c}_i \\ &= -\omega_i^2 \begin{bmatrix} \mathbb{I}_\pi & \mathbf{D}_{\pi\gamma} \\ \mathbf{D}_{\pi\gamma}^\dagger & \mathbb{I}_\gamma \end{bmatrix} \mathbf{c}_i, \end{aligned} \quad (1)$$

yielding mixed-mode angular frequencies ω_i and mixing coefficients c_{ij} as the resulting eigenvalues and eigenvectors, such that the mixed mode eigenfunctions are expressed as linear combinations of those of π and γ modes with these coefficients, as $\xi_{\text{mixed},i} = \sum_j c_{ij} \xi_j$. As in OB20, here Ω_π and Ω_γ are diagonal matrices whose entries are the squared angular frequencies of the π and γ modes, and \mathbb{I}_π and \mathbb{I}_γ are identity matrices of the same ranks as the number of π and γ modes under consideration.

We adopt most of the expressions from OB20 for these matrix elements: in particular, the volume integrals specifying the overlap terms

$$D_{\pi\gamma,ij} = \int \rho \xi_{\pi,i}^* \cdot \xi_{\gamma,j}^* d^3x, \quad (2)$$

where $\vec{\xi}$ is the Lagrangian displacement eigenfunction associated with a mode and ρ is the local density. Likewise, we use their expressions for the π -mode interaction terms:

$$R_{\pi\pi,ij} = \left\langle \xi_{\pi,i}, \hat{\mathcal{R}}_\pi \xi_{\pi,j} \right\rangle = - \int \rho N^2 \xi_{r,\pi,i}^* \xi_{r,\pi,j} d^3x, \quad (3)$$

where N^2 is the squared Brunt-Väisälä frequency. These expressions assume unit normalisation of the eigenfunctions with respect to the standard inner product:

$$\int \rho \xi_{\pi,i}^* \cdot \xi_{\pi,j} d^3x = \int \rho \xi_{\gamma,i}^* \cdot \xi_{\gamma,j} d^3x = \delta_{ij}. \quad (4)$$

For the γ -mode self-interaction terms $\mathbf{R}_{\gamma\gamma}$, we have derived new expressions that are manifestly Hermitian; this addresses a significant shortcoming in the OB20 construction. While essential to our subsequent numerical calculations, the derivation of these new expressions is not the central focus of this work, and we leave the details of it to Appendix A.

2.1. Perturbation Theory for the Generalised Hermitian Eigenvalue Problem

Given a perturbed Hermitian eigenvalue problem of the form

$$(\mathbf{H}_0 + \lambda \mathbf{V})\mathbf{c}_n = \varepsilon_n \mathbf{c}_n, \quad (5)$$

Rayleigh-Schrödinger perturbation theory permits a description of the perturbed eigenvalues ε_n and eigenvectors \mathbf{c}_n in terms of the eigensystem associated with the unperturbed operator \mathbf{H}_0 , in the form of an asymptotic series in powers of the parameter λ . We refer the reader to textbooks on linear algebra or quantum mechanics for reminders of the usual expressions, which we will reproduce here without proof: given

$$\varepsilon_n \sim \sum_k \lambda^k \varepsilon_n^{(k)}; (\mathbf{c}_n)_m \equiv c_{nm} \sim \sum_k \lambda^k c_{nm}^{(k)}, \quad (6)$$

the terms in this series expansion are found by expanding Eq. (6) into Eq. (5), collecting terms by powers of λ , and demanding that the perturbed eigenvectors be orthonormal. This results in a set of recurrence relations which yield at last that

$$\begin{aligned} \varepsilon_n &\sim \varepsilon_n^{(0)} + \lambda V_{nn} + \lambda^2 \left(\sum_{m \neq n} \frac{V_{nm} V_{mn}}{\varepsilon_n^{(0)} - \varepsilon_m^{(0)}} \right) + \mathcal{O}(\lambda^3), \\ c_{nm}^{(0)} &\sim \delta_{nm} + \lambda \frac{V_{nm}}{\varepsilon_n^{(0)} - \varepsilon_m^{(0)}} + \mathcal{O}(\lambda^2). \end{aligned} \quad (7)$$

However, with respect to the bare π and γ modes, Eq. (1) is a GHEP, where the right-hand-side of the equation (proportional to the eigenvalues) is also potentially affected by the perturbation: hence Eq. (7) is not directly applicable. We regroup terms, and rewrite the eigenvalues as $-\omega_i^2 \equiv \varepsilon_i$, to yield

$$\begin{aligned} (\mathbf{L}_0 + \kappa \mathbf{P} + \lambda \mathbf{V})\mathbf{c}_n &= \begin{bmatrix} \mathbf{E}_\pi + \kappa \mathbf{P}_{\pi\pi} + \lambda \mathbf{V}_{\text{surf}} & \kappa \mathbf{P}_{\pi\gamma} \\ \kappa \mathbf{P}_{\pi\gamma}^\dagger & \mathbf{E}_\gamma + \kappa \mathbf{P}_{\gamma\gamma} \end{bmatrix} \begin{bmatrix} \mathbf{c}_\pi \\ \mathbf{c}_\gamma \end{bmatrix} \\ &= -\omega_n^2 \begin{bmatrix} \mathbb{I}_\pi + \lambda \mathbf{Q}_{\text{surf}} & \kappa \mathbf{D}_{\pi\gamma} \\ \kappa \mathbf{D}_{\pi\gamma}^\dagger & \mathbb{I}_\gamma \end{bmatrix} \begin{bmatrix} \mathbf{c}_\pi \\ \mathbf{c}_\gamma \end{bmatrix} \equiv \varepsilon_n (\mathbf{1} + \kappa \mathbf{D} + \lambda \mathbf{Q}) \mathbf{c}_n. \end{aligned} \quad (8)$$

We have regrouped terms in order to treat κ and λ as two separate parameters, both taking values between 0 and 1. The parameter κ quantifies the overall coupling between the π and γ subsystems (described by the matrix \mathbf{P}). As we reduce to the uncoupled problem with $\kappa \rightarrow 0$, the matrix \mathbf{L}_0 on the LHS becomes diagonal; its elements are given by the oscillation frequencies of the bare π and γ modes. In the same limit, the ‘‘metric’’ matrix on the RHS reduces to the identity matrix. On the other hand, λ describes the size of a structural perturbation to the stellar model associated with some differential operator $\hat{\mathcal{V}}$; by convention, it also takes values between 0 and 1. For reasons that we will discuss in the following section, the matrices \mathbf{V} and \mathbf{Q} can be assumed to vanish outside the π -mode subspace when the perturbation represents the surface term; however this property is not essential to our subsequent discussion.

In principle, it is possible to choose some basis that diagonalises the matrix $(\mathbb{I} + \kappa \mathbf{D})$ on the RHS for any value of κ , permitting the direct use of Eq. (7); this is the strategy which was pursued in OB20. However, in this basis the diagonal elements of the LHS matrix \mathbf{L}_0 may lose their intuitive interpretations, as given above. Moreover, since numerically we only have access to incomplete matrices (as the underlying differential operators are of infinite rank), in practice this change of basis can only be performed approximately. This approximation must be performed to the same order of accuracy as the order to which the perturbative expansion itself is truncated. The resulting procedure becomes highly cumbersome very quickly beyond first order.

To avoid this, we perform a Rayleigh-Schrödinger-like expansion to an asymptotic series in λ in the usual fashion, under the assumption of dominant balance that $\kappa \sim \lambda$ (since formally both take values between 0 and 1). Conceptually, we are ‘‘turning on’’ both the mixed-mode coupling and the structural perturbation at the same time. This gives us the following explicit expressions:

- At zeroth order in λ we require $\varepsilon_n(\lambda = 0) = \varepsilon_n^{(0)}$ and $c_{nm}^{(0)} = \delta_{nm}$, as in Eq. (7).
 - At first order in λ we have
- $$\varepsilon_n^{(1)} = V_{nn} + P_{nn}; c_{nm}^{(1)} = \frac{V_{mn} + P_{mn}}{\varepsilon_n^{(0)} - \varepsilon_m^{(0)}} - D_{mn} - Q_{mn} \text{ for } m \neq n. \quad (9)$$

The self-mixing terms $c_{nn}^{(1)}$ are found by demanding that $\mathbf{c}_n^\dagger (\mathbf{1} + \lambda (\mathbf{D} + \mathbf{Q})) \mathbf{c}_n = 1 + \mathcal{O}(\lambda^2)$, yielding at last that $c_{nn}^{(1)} = -D_{nn} - Q_{nn} = -Q_{nn}$.

- Higher-order terms at k^{th} order in λ can be found recursively from those of lower order, through the recurrence relation

$$\begin{aligned} &(\varepsilon_n^{(0)} - \varepsilon_m^{(0)}) \left(c_{nm}^{(k)} + \sum_l A_{ml} c_{nl}^{(k-1)} \right) + \varepsilon_n^{(k)} \delta_{mn} \\ &= \sum_l B_{ml} c_{nl}^{(k-1)} - \sum_{j=1}^{k-1} \varepsilon_n^{(j)} \left(c_{nm}^{(k-j)} + \sum_l A_{ml} c_{nl}^{(k-j-1)} \right), \end{aligned} \quad (10)$$

to produce the eigenvalue perturbation $\varepsilon_n^{(k)}$ and eigenvector components $c_{nm}^{(k)}$ where $m \neq n$. Here we have written $A_{mn} = D_{mn} + Q_{mn}$ and $B_{mn} = V_{mn} + P_{mn}$ for brevity, since each pair of matrices appears together in Eq. (8). The constraint of orthonormality gives

$$\begin{aligned} 2\text{Re}(c_{nn}^{(k)}) + \sum_{l=1}^{k-1} \sum_m c_{nm}^{(l)*} c_{nm}^{(k-l)} + 2\text{Re} \left(\sum_m A_{nm} c_{nm}^{(k-1)} \right) \\ + \sum_{l=1}^{k-2} \sum_{j,m} c_{nj}^{(l)*} A_{jm} c_{nm}^{(k-l-1)} = 0, \end{aligned} \quad (11)$$

which then yields the self-mixing eigenvector components $c_{nm}^{(k)}$.

It can be seen that these recurrence relations reduce to the usual Rayleigh-Schrödinger expressions as $A_{ij} \rightarrow 0$.

2.2. The surface term as a matrix perturbation

The matrix construction of **OB20** associates linear operators $\hat{\mathcal{A}}$ with matrix elements A_{ij} with respect to some set of basis functions. These matrix elements are found by performing integrals of the form

$$A_{ij} = \langle \vec{\xi}_i, \hat{\mathcal{A}} \vec{\xi}_j \rangle = \int dm \vec{\xi}_i^* \cdot \hat{\mathcal{A}} \vec{\xi}_j, \quad (12)$$

i.e. using the inner product for which our chosen sets of basis functions — in this case, the isolated π and γ -mode eigenfunctions — are orthonormal. With respect to this construction, we now consider frequency perturbations associated with the surface term to result from a perturbation to the wave operator of the form

$$\hat{\mathcal{L}} \rightarrow \hat{\mathcal{L}} + \lambda \hat{\mathcal{V}}. \quad (13)$$

The operator $\hat{\mathcal{V}}$ carries the following interpretation: we consider two different stellar structures, which we constrain to have identical global properties (in particular, identical mass and radius). We assume we have access to the eigensystem of one of them, which is associated with the wave operator $\hat{\mathcal{L}}$; we treat this as our fiducial structure (or reference model, in the parlance of helioseismology). The second stellar structure has a different set of pulsation frequencies and eigenfunctions, associated with a different wave operator, which we write as $\hat{\mathcal{L}} + \hat{\mathcal{V}}$, acting on the same domain. The parameter λ , taking values in the range $[0, 1]$, serves to interpolate between the two structures. In this manner, we may express differences between two stellar structures as a classical operator (and therefore matrix) perturbation problem, parameterised by λ .

Accordingly, characterising the surface term within this matrix construction requires computing the matrix elements of $\hat{\mathcal{V}}$ via Eq. (12), with respect to the basis set of eigenfunctions from the fiducial model. If $\hat{\mathcal{V}}$ represents the surface term — i.e. the structural difference compared to our fiducial model is localised to the stellar surface — then by assumption, we should also have

$$\hat{\mathcal{V}} \sim \delta(r-R) \implies \hat{\mathcal{V}} \xi_{\gamma,i} \rightarrow 0, \quad (14)$$

since γ modes are confined to the stellar interior, and thus in principle are unaffected by the surface term. By an analogous argument, it can be shown that the matrix elements Q_{ij} also vanish when evaluated with respect to γ -modes.

Based on these properties, we now construct an analogous parametrisation to **BG14** within this matrix formalism. In particular, we observe that the diagonal elements of Eq. (1) can be rewritten as integrals of the form

$$\omega_i^2 \int dm \vec{\xi}_i \cdot \vec{\xi}_i + \int dm \vec{\xi}_i \cdot \hat{\mathcal{L}} \vec{\xi}_i = 0. \quad (15)$$

Not coincidentally, this is precisely the same structure as the “variational” construction employed by **Lynden-Bell & Ostriker (1967)** and subsequently by **Gough (1990)**, neglecting

the rotational splitting term, from which **BG14** derive their ansatz parametrisation. In recovering frequency perturbations from such integrals, these approaches restrict consideration to only the diagonal elements of the matrix construction.

Obversely, we know that the diagonal elements of the perturbation matrix completely specify the perturbations to the frequency eigenvalues only to first order in the Rayleigh-Schrödinger expansion; cf. Eq. (7). The variational analysis presented by **Gough (1990)** and elsewhere can therefore be interpreted as the truncation of the perturbative expansion for the frequency eigenvalues to leading order in the expansion parameter λ . Conversely, any generalisation to this first-order approach must require that the off-diagonal matrix elements be specified. Retracing the arguments of **Gough (1990)** (in particular, that $\nabla \cdot \vec{\xi}_i \sim \omega^2 \xi_{i,r}$ and $\xi_r \sim |\xi|$ near the stellar surface), we find that perturbations to the stellar model localised at the stellar surface result in perturbation matrix elements of the form

$$V_{ij} \sim \left(\oint d\Omega \vec{\xi}_i^*(R) \cdot \vec{\xi}_j(R) \right) \left(a + b \left(\frac{\omega_i^2 \omega_j^2}{\omega_0^4} \right) \right), \quad (16)$$

for some constants a, b, ω_0 . This is a bilinear form in the frequency eigenvalues, which reduces to the quadratic form derived in **Gough (1990)** when evaluated along the diagonal elements. The two coefficients a, b here correspond to the parameters a_{-1}, a_3 of **BG14**, which takes the form

$$\delta v_{nl} \sim v_0 \left(a_{-1} \left(\frac{v_{nl}}{v_0} \right)^{-1} + a_3 \left(\frac{v_{nl}}{v_0} \right)^3 \right) \Big| I_{nl}. \quad (17)$$

In terms of those parameters, we may equivalently write

$$V_{ij} \sim -2\omega_0^2 \left(a_{-1} + a_3 \left(\frac{\omega_i^2 \omega_j^2}{\omega_0^4} \right) \right) \Big| \sqrt{I_i I_j}, \quad (18)$$

which is the appropriate matrix generalisation of the correction of **BG14**. We note that γ -mode eigenfunctions are evanescent outside of the central buoyant cavity, so this construction also approximately satisfies Eq. (14). In a similar manner, we find that

$$Q_{ij} = \oint d\Omega \delta\rho(R) \vec{\xi}_i^*(R) \cdot \vec{\xi}_j(R), \quad (19)$$

where $\delta\rho$ is the static localised perturbation to the density profile associated with the surface term. This term gives rise to a contribution to the frequency perturbation that goes as $\delta\omega_{nl} \sim \omega_{nl}/I_{nl}$, which is usually assumed to be negligible in analyses of the surface term. We will also neglect it in our subsequent discussion.

While we have limited ourselves to considering only structural perturbations, to preserve the analogy with **Gough (1990)**; **Ball & Gizon (2014)**, we note that this matrix construction is not strictly limited to them. For example, interactions with a magnetic field or a nonzero fluid velocity field may also result in additional force terms in the momentum equation.

In such cases, the linearised contributions of these terms in the time-independent wave equation, Eq. (A7), take the form of additional differential operators acting on the wavefunctions (e.g. Lynden-Bell & Ostriker 1967; Gough & Thompson 1990), perturbing the fiducial system in a similar manner. Their associated matrix elements can also be found by evaluating volume integrals per Eq. (12), and the above analysis can then be applied wholesale (up to modified parameterisation), potentially also incorporating additional dependences on the azimuthal order m through a quadratic variant of the GHEP (cf. Ong & Basu, in prep.). However, the details of how these matrix corrections are parametrised will still depend on the physical assumptions being made, just as is the case with pure p -modes. It is precisely for this reason that a nonparametric surface-term diagnostic remains desirable.

2.3. Convergence of the perturbative expansion

A formal expansion in powers of λ yields good approximations only if the perturbation is heuristically “small”, since the resulting series is asymptotic but not necessarily convergent. On the other hand, as we have just discussed, using only diagonal matrix elements to describe the surface term coincides with the truncation of this series expansion to leading order in λ . This is more generally also true of any result obtained with “variational” methods. Therefore, determining the conditions under which this perturbative expansion converges will also illuminate the limits of validity for these existing methods.

To proceed, we need to first establish some properties of the perturbation coefficients $\varepsilon_n^{(k)}$. When the coupling is weak enough to allow us to neglect the overlap terms D_{ij} , we may recycle standard expressions that apply to the Rayleigh-Schrödinger expansion Eq. (7), with B in place of V . By inspection of Eq. (10), it can be shown that for $k > 2$, these can be written as a sum in powers of B_{nm} :

$$\begin{aligned} \varepsilon_n^{(k)} &\sim (-B_{nm})^{k-2} \sum_{m \neq n} \frac{|B_{nm}|^2}{(\varepsilon_n^{(0)} - \varepsilon_m^{(0)})^{k-1}} \\ &+ (-B_{nm})^{k-3} \sum_{m_1, m_2 \neq n} \sum_{l=1}^{k-1} \frac{B_{nm_1} B_{m_1 m_2} B_{m_2 n}}{(\varepsilon_n^{(0)} - \varepsilon_{m_1}^{(0)})^l (\varepsilon_n^{(0)} - \varepsilon_{m_2}^{(0)})^{k-l-1}} \\ &\vdots \\ &+ \sum_{m_1 \neq n} \cdots \sum_{m_{k-1} \neq n} \frac{B_{nm_1} B_{m_1 m_2} \cdots B_{m_{k-1} n}}{(\varepsilon_n^{(0)} - \varepsilon_{m_1}^{(0)}) \cdots (\varepsilon_n^{(0)} - \varepsilon_{m_{k-1}}^{(0)})}. \end{aligned} \quad (20)$$

Let us first consider the case of a surface perturbation acting on p -modes, or bare π -modes, where Eq. (7) describes the perturbative expansion; correspondingly we use Eq. (20) with V in place of B . Since these are typically observed at high radial order ($n_p \gtrsim 10$), the relative change in the matrix elements V_{nm} , keeping n fixed, is small as we move off the diagonal, compared to the relative changes in the resonance terms $\varepsilon_n^{(0)} - \varepsilon_m^{(0)}$. Accordingly, we approximate $V_{nm} \sim V_{nn}$ near the diagonal. At the same time, this sum is also domi-

nated by terms near the diagonal, since off-diagonal terms are otherwise heavily suppressed by the resonance factors in the denominator. For any given p or π -mode, we have

$$\left| \varepsilon_n^{(k)} \right| \lesssim k^q \max_{m \neq n} \left| \frac{V_{nm}^k}{(\varepsilon_n^{(0)} - \varepsilon_m^{(0)})^{k-1}} \right| \sim \frac{k^q |V_{nn}|^k}{\left| \min_{m \neq n} (\varepsilon_n^{(0)} - \varepsilon_m^{(0)}) \right|^{k-1}}, \quad (21)$$

where k^q counts the number of such terms that survive the summation over alternating signs. If we neglect the alternating signs, we have $q \sim 2$, which bounds the sum from above. However, the smallest possible separation between p -modes or π -modes in the asymptotic regime is roughly given by $\Delta\nu$. Writing $V_{nm} \sim \delta\omega_q^2 \sim 2\omega_n \cdot 2\pi\delta\nu_{\text{surf}}$, we find

$$\left| \varepsilon_n^{(k)} \right| \lesssim k^2 \cdot |V_{nn}| \cdot \left(\frac{\delta\nu_{\text{surf}}}{\Delta\nu} \right)^{k-1}. \quad (22)$$

In practice, the size of the frequency perturbation from the surface term is small enough that it may also be expressed as a phase shift in the eigenvalue equation (i.e. a small fraction of $\Delta\nu$). The ratio in the parentheses is then, by assumption, much less than 1, and this series can be shown to converge via e.g. the integral test.

Turning our attention to mixed modes, we split our analysis into two cases by comparing the matrix elements of \mathbf{V} and \mathbf{P} . Since the surface term leaves γ modes unaffected, following our discussion in Section 2.2, we have $V_{ij} \ll P_{ij}$ where i indexes a π mode and j a γ mode. Where the coupling is strong, we also have $V_{i_1 i_2} \ll P_{i_1 i_2}$ for all modes i_n in the π -mode subspace. Since we cannot neglect the mode coupling in these cases, we cannot use Eq. (20) directly. Instead we must consider the coupled system (including the avoided crossing) to be our fiducial set of eigenvalues and eigenfunctions, so that the perturbative series is described by Eq. (7), and we again use Eq. (20) with V in place of B . A further complication is that the matrix elements of V must now be evaluated with respect to the mixed-mode rather than bare π -mode system. Once again we approximate $V_{i_1 i_2} \sim V_{i_1 i_1}$ within the π -mode subspace. For π -dominated mixed modes, this leads us to also approximate $V_{mm} \sim V_{nn}$, whence we again obtain Eq. (21).

In this case, however, the minimum distance between eigenvalues is not solely determined by the asymptotic properties of the underlying eigenvalues, since there are two sets of underlying asymptotic relations which evolve independently of each other. Instead, as modes from the π set come into resonance with modes from the γ set, the minimum separation between modes in the resulting avoided crossing will be determined by the coupling strength. This coupling strength is a function of the mode frequency, which (assuming it varies slowly with frequency) we approximate as some constant P . Conversely, if a resonant pair exists, then for each of them the sum over terms in Eq. (20) will be dominated by resonance terms involving the other. Therefore, in these cases we obtain as our condition for convergence that

$$\left| \varepsilon_n^{(k)} \right| \lesssim k^2 \cdot |V_{nn}| \cdot \left(\frac{\delta\nu_{\text{surf}}}{P/8\pi^2\nu_\pi} \right)^{k-1} \implies \frac{\delta\nu_{\text{surf}}}{P/8\pi^2\nu_\pi} \ll 1. \quad (23)$$

But this is essentially a restatement of our original condition for performing this analysis in the first place — i.e. that the coupling strength is large compared to the surface term. That is to say, this sum always converges in the case of strong coupling. This is a sufficient but not necessary condition, in that, conversely, the series need not necessarily diverge for $V_{mn} \gtrsim P$.

Finally, in the opposite case of weak coupling, $V_{i_1 i_2} \gg P_{i_1 j}$, and we may use Eq. (20) directly. On the diagonal, $B_{ii} = V_{ii}$, while off the diagonal, $B_{ij} = P_{ij}$. Moreover, since the coupling is weak, the perturbative expansion Eq. (20) is dominated by terms containing the highest powers of the diagonal elements. For $k > 2$ we then have

$$\begin{aligned} \varepsilon_n^{(k)} &\sim (-1)^k \sum_{m \neq n} \frac{(V_{mn})^{k-2} |P_{mn}|^2}{(\varepsilon_n^{(0)} - \varepsilon_m^{(0)})^{k-1}}, \\ c_{nm}^{(k)} &\sim (-1)^k \frac{(V_{mn})^{k-1} P_{mn}}{(\varepsilon_n^{(0)} - \varepsilon_m^{(0)})^k}. \end{aligned} \quad (24)$$

Since the eigenvalues are now given by the bare π and γ modes, the spacing between them is in principle not bounded from below (because the bare π and γ eigenvalues may cross freely over the course of stellar evolution). Conversely, it is in general bounded from above by $\min(\Delta\nu, \nu^2 \Delta\Pi)$. In the weak coupling regime in particular, we moreover have $\nu^2 \Delta\Pi < \Delta\nu$. Accordingly, the perturbation coefficients are bounded from below as

$$|\varepsilon_n^{(k)}| \gtrsim \frac{P^2}{|V_{mn}|} \cdot \left(\frac{\delta\nu_{\text{surf}}}{\nu^2 \Delta\Pi} \right)^{k-1}. \quad (25)$$

Note that the direction of the inequality is now reversed: we have derived that this series *fails to converge* if $\delta\nu_{\text{surf}} > \nu^2 \Delta\Pi$. Again, the converse is not necessarily true (i.e. the series may not necessarily converge even if $\delta\nu_{\text{surf}} < \nu^2 \Delta\Pi$). Comparing values of $\Delta\Pi$ and the coupling strength as computed from models reveals that the two quantities roughly scale with each other over the course of stellar evolution. Consequently this condition and Eq. (23) are mutually exclusive (see our subsequent description of Fig. 1).

There is one final asymptotic regime under which we may once again rely on perturbation theory even where this series diverges. Ball et al. (2018), OB20, and Ong et al. (2021) show that if $\Delta\nu \gg \nu^2 \Delta\Pi \gg P/8\pi^2\nu$, then the density of π -modes is so high, and the π - γ coupling is so weak, that the p -dominated mixed mode frequencies which emerge are well-approximated by those of pure π -modes. In these cases we may safely treat the effects of the surface term on the observed modes as we would if they were bare π -modes, and ignore the details of mode coupling altogether. This is already common practice for treating the quadrupole modes of evolved red giants.

In summary: the traditional ‘‘variational’’ analysis, from which the BG14 surface term is derived, always holds good when applied to p -modes or bare π -modes. However, such analyses cannot always be applied to mixed modes. We have shown that if the frequency shift within the bare π -mode subspace

is given by $\delta\nu_{\text{surf}}$, then these constructions may only be applied to mixed modes where it is smaller than the smallest separation between adjacent modes. This may be variously specified by $\Delta\nu$, the relative coupling strength $P/8\pi^2\nu$, or the local γ -mode spacing $\nu^2 \Delta\Pi$ at different stages of the evolution of the star off the main sequence. These bounds follow from quite general considerations, which also will apply to other contexts where such variational constructions are typically invoked (e.g. in the construction of structural or rotational inversion kernels).

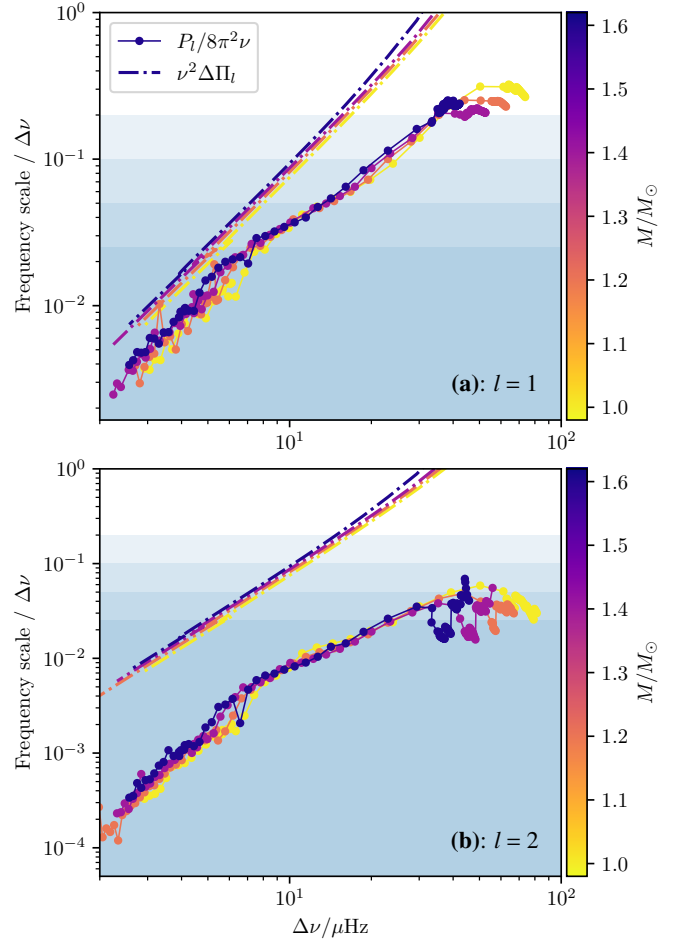


Figure 1. Evolution of the mixed-mode coupling strength $P/8\pi^2\nu$ (points connected with lines) and γ -mode separation $\nu^2 \Delta\Pi_l$ (dashed-dotted lines) in the neighbourhood of ν_{max} for evolutionary tracks of solar composition. We show these quantities as computed for (a) dipole ($l = 1$) and (b) quadrupole ($l = 2$) modes. The shaded regions indicate constant fractions of $\Delta\nu$ (see text).

To illustrate these various regimes of approximation, we plot in Fig. 1 the relative coupling strength $P/8\pi^2\nu$ (found by averaging matrix elements near ν_{max}), and the local γ -mode separation $\nu^2 \Delta\Pi$, as computed with respect to MESA models with solar-calibrated α_{MLT} and Y_0 , on evolutionary tracks with the GS98 element mixture at solar metallicity. For this

purpose we use the same evolutionary tracks as in [Ong & Basu \(2019\)](#). However, following [Benomar et al. \(2012\)](#) (who used an approximate parametrisation of the coupling strength), we expect these quantities to at least qualitatively be independent of the composition of the stellar models. We show these quantities as averaged over π and γ modes within $4\Delta\nu$ of ν_{\max} , in units of $\Delta\nu$. We compute these quantities for evolutionary tracks with stellar masses between 1 to $1.6 M_{\odot}$, from the onset of mode mixing (i.e. where the lowest-order γ mode enters into the frequency range of interest) to past the RGB bump.

Since the surface term frequency perturbation $\delta\nu_{\text{surf}}$ is typically assumed to be a small fraction of $\Delta\nu$, we mark out the constant multiples 0.2, 0.1, 0.05 and $0.025\Delta\nu$ with the horizontal shaded regions. The different regimes of convergence we have described can be read off immediately from these diagrams for any choice of $\delta\nu_{\text{surf}}$. For example: with $\delta\nu_{\text{surf}} \sim 0.1\Delta\nu$ near ν_{\max} , we find that first-order constructions like that of [BG14](#) are only reliable for dipole modes where $\Delta\nu \gtrsim 20 \mu\text{Hz}$, while no perturbative treatment is valid for $\Delta\nu \lesssim 10 \mu\text{Hz}$. For $\Delta\nu \lesssim 20 \mu\text{Hz}$, however, we also see that, since the quadrupole coupling strength is orders of magnitude weaker, we may neglect mode mixing altogether for quadrupole and higher-degree modes.

3. ϵ -MATCHING

While parametrisations like that of [BG14](#) can be expressed globally (i.e. as closed-form integrals over the stellar structure), the so-called ϵ -matching algorithm, which we describe below, operates on the partial-wave phase functions of the pulsation eigenfunctions, and does not as easily admit such a global description.

For pure p or π modes, the radial displacement wavefunctions of partial waves at angular frequency ω may be approximated near the centre of the star with spherical Bessel functions as

$$\xi_{r,l}(\omega, t) \sim A_l(\omega, t) j_l(\omega t - \delta_l(\omega, t)), \quad (26)$$

where A_l is an inner amplitude function, δ_l is the inner phase function, and $t = \int_0^r dr/c_s$ is the acoustic radial coordinate. A similar approximation can be made near the outer boundary of the star, with corresponding outer amplitude and phase functions B_l and α_l . Further self-consistency requirements ([Calogero 1963](#); [Babikov 1976](#)) permit α_l and δ_l to be specified uniquely, up to integer multiple of π , by integrating a set of nonlinear ordinary differential equations starting from the outer and inner boundaries, respectively. [Roxburgh \(2015\)](#) showed that both α_l and δ_l tend towards fixed values when evaluated at suitable matching points $t_0, 0 < t_0 < T$, sufficiently far from both the inner and outer boundaries at $t = 0$ and $t = T$; their values there may be treated as functions of frequency alone. When ω is the angular frequency of a normal mode, they must also satisfy the eigenvalue equation

$$\omega_{nl}T + (\alpha_l(\omega_{nl}) - \delta_l(\omega_{nl})) \equiv \omega_{nl}T - \pi\epsilon_l(\omega_{nl}) = n\pi. \quad (27)$$

Since the stratification in the outer layers of the star is approximately plane-parallel, the outer phase functions α_l do not

change significantly with l at low degree. [Roxburgh \(2016\)](#) exploited this property to devise a procedure for nonparametric diagnosis of the surface term, by comparing values of ϵ_l associated with model and observed frequencies (whence the name ϵ -matching). We generalise the approach in this section to account for mode mixing, both at first order in the coupling strength, as well as in more general cases.

Ordinarily, the ϵ -matching algorithm acts on observables of the form

$$\mathcal{E}_l(\nu_{l,n}^{\text{obs}}) = \epsilon_{l,n}^{\text{obs}} - \epsilon_l^{\text{mod}}(\nu_{l,n}^{\text{obs}}), \quad (28)$$

which we rewrite in terms of frequency differences as

$$\begin{aligned} \mathcal{E}_l(\nu_{l,n}^{\text{obs}}) &= \epsilon_{l,n}^{\text{obs}} - \epsilon_l^{\text{mod}}(\nu_{l,n}^{\text{mod}}) + \epsilon_l^{\text{mod}}(\nu_{l,n}^{\text{mod}}) - \epsilon_l^{\text{mod}}(\nu_{l,n}^{\text{obs}}) \\ &= \frac{\nu_{l,n}^{\text{obs}} - \nu_{l,n}^{\text{mod}}}{\Delta\nu} + (\epsilon_l^{\text{mod}}(\nu_{l,n}^{\text{mod}}) - \epsilon_l^{\text{mod}}(\nu_{l,n}^{\text{obs}})). \end{aligned} \quad (29)$$

Following our discussion in the previous section, the perturbation to the frequencies from the surface term results in a perturbation to the π subsystem alone, and we assume it to leave the γ -mode frequencies unchanged. In the presence of mode mixing, this means (replicating conventional wisdom) that γ -dominated modes are less strongly affected by the surface term than are π -dominated ones.

3.1. First-order construction

Let us first consider a mixed mode such that:

- i. Only a single π mode is significantly coupled to the γ -mode system. The mode eigenfunctions can then be written in the form

$$\xi_{\text{mixed},i} = c_{\pi,i}\xi_{\pi,i} + \sum_j c_{\gamma,ij}\xi_{\gamma,j}. \quad (30)$$

- ii. The frequency perturbation from the surface term is such that the coefficients c_{π} and c_{γ} are not significantly affected. This means that the surface term does not modify which π and γ modes happen to be in resonance.
- iii. The diagonal elements of the perturbation matrix are sufficient to specify the effect of the surface term on the π -mode subspace. We write this frequency shift from the surface term as $V_{ii} \equiv -\delta\omega_{\pi,i}^2$.

For a mixed mode satisfying these conditions, retaining terms to leading order in the perturbation gives us that

$$\delta\omega_{\text{mixed},i}^2 \sim \delta\omega_{\pi,i}^2 c_{\pi,i} \left(c_{\pi,i} + \sum_j c_{\gamma,ij} D_{ij} \right) \sim \delta\omega_{\pi,i}^2 / Q_{\text{mixed}}, \quad (31)$$

where $Q_{\text{mixed}} = I_{\text{mixed}}/I_{\pi,i}$ is the ratio between the mode inertia of the mixed mode and that of its underlying π mode. In the second step we have dropped the overlap terms D_{ij} . If this frequency perturbation is sufficiently small, we then have

$$\delta\nu_{\pi,i} \sim Q_{\text{mixed}} \cdot \delta\nu_{\text{mixed}}. \quad (32)$$

Accordingly, we obtain

$$\begin{aligned} \mathcal{E}_{\pi,l}(v_{l,n}^{\text{obs}}) &= \epsilon_{\pi,l,n}^{\text{obs}} - \epsilon_{\pi,l}^{\text{mod}}(v_{l,n}^{\text{obs}}) \\ &\sim \left(\frac{v_{l,n}^{\text{obs}} - v_{l,n}^{\text{mod}}}{\Delta v} \right) Q_{ln} + \left(\epsilon_{\pi,l}^{\text{mod}}(v_{l,n}^{\text{mod}}) - \epsilon_{\pi,l}^{\text{mod}}(v_{l,n}^{\text{obs}}) \right). \end{aligned} \quad (33)$$

For two stellar structures that differ only in their outer layers, this can be related to the differences between their outer partial-wave phase functions, in the same way as [Roxburgh \(2016\)](#):

$$\mathcal{E}_{\pi,l}(v_{l,n}^{\text{obs}}) \sim \alpha_{\pi,l}^{\text{obs}}(v_{l,n}^{\text{obs}}) - \alpha_{\pi,l}^{\text{mod}}(v_{l,n}^{\text{obs}}), \quad (34)$$

which should as usual collapse to a single function of frequency, $\mathcal{F}(v)$. Since the π -mode isolation condition is only applied in the interior of the star, $\alpha_{\pi}(v) \sim \alpha_p(v)$, hence this expression can also be applied to radial modes using interpolants constructed from the (technically inequivalent) uncoupled p -modes.

Therefore, this yields the following modified ϵ -matching procedure:

1. We match model and observed modes pairwise, assuming some reasonable mode identification.
2. For each mode pair, the quantity $\mathcal{E}_{\pi,l,n}$ in Eq. (33) is evaluated. We treat these as samples of some function $\mathcal{E}_{\pi,l}(v_{n,\text{obs}})$ evaluated at the observed frequencies.
3. The best-fitting model is the one for which these different sets of samples collapse to a single function of frequency, such that $\mathcal{E}_{\pi,l}(v) = \mathcal{F}(v)$ independently of l . As in [Roxburgh \(2016\)](#), we characterise this by way of a reduced- χ^2 cost function

$$\chi_{\epsilon}^2 = \min_{M_i, \{\theta_i\}} \frac{1}{N - M_i - 1} \sum_{l,n} \left(\frac{\mathcal{E}_l(v_{l,n}^{\text{obs}}) - \mathcal{F}(v_{l,n}^{\text{obs}}, \{\theta_i\})}{\sigma_{\mathcal{E}_l}} \right)^2, \quad (35)$$

where M_i counts the number of free parameters θ_i used in the fit to constrain $\mathcal{F}(v)$.

This procedure acts on pairwise frequency differences rather than on the phase functions, which cannot be directly estimated from the observed frequencies. At the same time, the explicit dependence on the π -mode phase function of the fiducial model eliminates the degeneracy under homology transformations that would otherwise emerge when considering only frequency differences. This works in much the same way as described for the original construction of [Roxburgh \(2016\)](#).

Since $I_{\pi,i} = I_{\pi}(v_i)$ is, for low-degree modes, a degree-independent function of frequency, Eq. (32) suggests that surface term treatments of the form $v_{\pi} \mapsto v_{\pi} + f(v_{\pi})$ can be modified for use with this restricted class of mixed modes as $v_i \mapsto v_i + [f(v_i)I_{\pi}(v_i)]/I_i$, where the quantity in the square brackets is itself a function of frequency. Conversely, any such inertia-weighted correction is implicitly also only applicable to mixed modes satisfying the criteria (i) and (ii) that we have

laid out above, whether or not the perturbation-theory considerations we have discussed in [Section 2.3](#) were explicitly invoked in its construction.

We now identify several sources of systematic error arising from approximations made in this construction, and attempt to provide rough estimates of their relative importance. Notably, we have made much stronger explicit assumptions in deriving this procedure than are made for most parametric methods. First, we have assumed that the coefficients $c_{i,\pi}^2$ can be reasonably approximated with $1/Q$; under unit normalisation, we have

$$Q = \frac{I}{I_{\pi,i}} \sim \frac{\oint d\Omega |\xi^{\vec{z}}(R)_{\pi,i}|^2}{\oint d\Omega |c_{\pi,i} \xi^{\vec{z}}(R)_{\pi,i} + \sum_j c_{\gamma,ij} \xi^{\vec{z}}(R)_{\gamma,j}|^2} \sim \frac{1}{c_{\pi,i}^2}, \quad (36)$$

where I is the mode inertia. This expression is exact only if the γ -mode eigenfunctions vanish at the surface. This is also implicit in the assumption that the surface term does not affect the γ modes.

Whereas we might apply mechanical boundary conditions that force the γ -mode eigenfunctions to vanish at the surface when solving for γ -modes (as done in [Ong & Basu 2020](#)), the g-like components of actual mixed modes are more closely described by those returned under more standard boundary conditions (e.g., vanishing Lagrangian pressure perturbation at the surface). The corresponding inertiae are finite, if large, and decrease with increasing frequency; equivalently, $|\xi_{\gamma,i}^{\vec{z}}(R)|$ is small, but increases with frequency. Nonetheless, even then we will expect that $\xi_{\gamma} \sim r^{-l-2}$ within the convective region as we approach the surface (e.g. [Pontin et al. 2020](#)), so we do not expect this to be significant.

Moreover, in Eq. (31), we have further assumed that the overlap integrals D_{ij} can be neglected. A priori, we expect this to hold in the asymptotic limit of high n_{γ} , but in this case we wish to apply this construction to the regime of isolated avoided crossings, which involve γ -modes of low radial order. More generally, we expect these overlap integrals to scale with the coupling strength $R_{\pi\gamma,ij}$ between the π and γ modes. This coupling strength is largest at low n_{γ} and low l , since this is where the π -modes penetrate most deeply, and the γ -modes decay the most slowly into the convection zone. Consequently, the errors incurred by this approximation will be largest in the regime of isolated low-degree avoided crossings — unfortunately, precisely where we intend to use this construction. However, even in this worst case, our subsequent calculations with stellar models indicate that we should not expect D_{ij} to be much larger than $\approx 10^{-1}$.

A more fundamental assumption going into this construction is item (ii), which requires that the π -mode mixing coefficient c_{π} not differ significantly between each of the observed and model mixed modes. This is equivalent to demanding that the inertia ratio Q of the mixed mode in the actual star is similar to that of the model mixed mode. Following our discussion in [Section 2.1](#), this assumption only holds good to first order in the surface perturbation, where the mixing coefficients are

left unchanged. Given the discussion in [Section 2.3](#), this construction is applicable to either p -dominated mixed modes which are far away from resonance with any γ -modes in both the star and the model, or for mixed modes in avoided crossings where the frequency shift from the surface term, $\delta\nu_{\text{surf}}$, is much smaller than the coupling strength of the avoided crossing. Consequently, this particular assumption holds best in the strong-coupling limit — i.e. in the same regime for which D_{ij} is largest.

In summary, for this construction to work well, we require that (I) $D_{ij} \ll 1$, and that (II) $\delta\nu_{\text{surf}}^2$ is small enough that first-order perturbation theory may be applied. Condition (I) holds best at high n_γ and high l , but is expected to incur only minor errors, while (II) holds best in the converse limit of low n_γ and low l .

3.2. The case of many π -modes per mixed mode

The assumption (i) underlying the above construction is equivalent to demanding an injective mapping from mixed modes to π -modes, in the sense that each mixed mode is uniquely associated with a single π mode. This enters into our final expression for the phase difference function, Eq. (33), via the inertia ratio Q . In the general case where

$$\xi_{\text{mixed},k} = \sum_i c_{\pi,ki} \xi_{\pi,i} + \sum_j c_{\gamma,kj} \xi_{\gamma,j}, \quad (37)$$

we instead obtain (again neglecting the π - γ overlap terms)

$$\delta\omega_{\text{mixed},k}^2 \sim \sum_i \delta\omega_{\pi,i}^2 c_{\pi,ki}^2. \quad (38)$$

Solving for the pure π -mode frequency perturbations will require inverting the corresponding mixed-mode squared-coefficient matrix, which cannot easily be related to traditional quantities like the mode inertiae. That is, we can no longer relate $c_{\pi,ki}$ to Q_k . This approach will strictly only be necessary if the coupling strength between the π and γ mode cavities is very strong, so that $\Delta\nu \ll P/8\pi^2\nu$. However, we see from [Fig. 1](#) (and accompanying discussion) that this is never the case within the observational regime of interest. Therefore, while a generalisation of our procedure to permit such cases is possible in principle, in practice it will never be necessary.

3.3. Generalised cost function

Ultimately, we seek to generalise this procedure to cases where condition (ii) does not hold, which (per our discussion in [Section 2.3](#)) is necessary for evolved stars where $\delta\nu_{\text{surf}} > \nu^2\Delta\Pi$. In such cases, perturbation theory cannot be relied upon, and we must seek recourse to explicitly solving the coupled matrix problem, Eq. (1). In general, the recovery of the perturbed π -mode frequencies from the surface-perturbed mixed modes is an underdetermined problem where we cannot rely on the coefficient matrices to remain approximately constant. Therefore, in these cases we cannot use these modes to directly constrain the best-fitting phase-difference function $\mathcal{F}(\nu)$.

However, from [Fig. 1](#) we can see that the coupling strength for quadrupole modes is orders of magnitude weaker than for dipole modes. Since the classical inner turning points of π -modes at fixed frequency scale as $r_t \sim \sqrt{l(l+1)}$, we expect the coupling at higher degree to be weaker still. Accordingly, in some cases we may ignore the effects of mode coupling on the quadrupole (and higher degree) modes, but not dipole modes. In such cases we may then use the radial and quadrupole (and potentially higher-degree) modes to first constrain $\mathcal{F}(\nu)$ separately, and then compute a cost function from the dipole modes by performing the appropriate implied correction on the π -mode subsystem.

Let us suppose that we have already constrained $\mathcal{F}(\nu)$ in this manner, using N_ϵ out of N_{tot} observed modes. As in Eq. (29), if the difference between the two sets of mode frequencies is only the result of the surface term, then applying a surface-term correction to the model π -mode frequencies $\nu_{\pi,\text{mod}}$ should yield a new set of frequencies $\nu_{\pi,\text{surf}}$, which must satisfy

$$\frac{\nu_{\pi,\text{surf}} - \nu_{\pi,\text{mod}}}{\Delta\nu} + \epsilon_\pi^{\text{mod}}(\nu_{\pi,\text{mod}}) - \epsilon_\pi^{\text{mod}}(\nu_{\pi,\text{surf}}) = \mathcal{F}(\nu_{\pi,\text{surf}}). \quad (39)$$

This is an implicit equation for $\nu_{\pi,\text{surf}}$, which must be solved numerically. If we make the further assumption that $\nu_{\pi,\text{surf}} - \nu_{\pi,\text{mod}}$ is small, we may approximate $\nu_{\pi,\text{surf}}$ in closed form by Taylor-expanding Eq. (39) to first order around ν_{mod} , to obtain

$$\nu_{\pi,\text{surf}} \sim \nu_{\pi,\text{mod}} + \frac{\mathcal{F}(\nu_{\pi,\text{mod}})}{\left. \frac{1}{\Delta\nu} - \frac{\partial}{\partial\nu} (\epsilon_\pi^{\text{mod}} + \mathcal{F}) \right|_{\nu_{\pi,\text{mod}}}}. \quad (40)$$

Once a full set of $\nu_{\pi,\text{surf}}$ is obtained, we then modify the diagonal elements of the matrix \mathbf{L}_π associated with the π -mode system of the fiducial model. The resulting surface-perturbed mixed modes associated with the model may then be computed by solving Eq. (1) for the mixed-mode eigenvalues. These mixed modes yield an auxiliary cost function of the usual form:

$$\chi_{\text{matrix}}^2 = \sum_i \left(\frac{\nu_{\text{obs},i} - \nu_{\text{mixed,surf},i}}{\sigma_i} \right)^2. \quad (41)$$

The cost function to be associated with the model is then given by combining contributions from the ϵ -matching proper and these extra terms:

$$\chi_{\text{tot}}^2 = \frac{1}{N_{\text{tot}} - M - 1} (\chi_{\text{matrix}}^2 + (N_\epsilon - M - 1)\chi_\epsilon^2). \quad (42)$$

4. TESTS USING STELLAR MODELS

We test the constructions in [Section 3](#) with simple injection-recovery test cases, using stellar models constructed with MESA (Paxton et al. 2011, 2013, 2018), with their mode frequencies and coupling matrices computed with GYRE (Townsend & Teitler 2013). We compute mode frequencies in the interval $[\nu_{\text{max}} - \nu_0 - \Delta\nu, \nu_{\text{max}} + \nu_0]$ such that the upper limit of this interval is set by the maximum value of the acoustic

cutoff frequency in the atmosphere of the fiducial model. This interval is used for computing both the mixed modes proper, as well as all of the π modes necessary to compute the matrices in Eq. (1). For the γ -mode system, we instead compute all modes in the interval $[\nu_{\max} - \nu_0 - 2\Delta\nu, \max_{r < 0.9R} N/2\pi]$, in order to make the coupling matrices which appear in Eq. (1) sufficiently complete for quantitative use.

To simulate a surface term, we introduce a structural perturbation to our chosen fiducial models, and for these perturbed models compute only the resulting mixed-mode frequencies (i.e. we do not permit ourselves access to the underlying decoupled π and γ systems). For these demonstrations, the precise form of this perturbation is not important, as long as it is localised to the surface. We choose a surface perturbation of the form $P \mapsto P(1 + \Delta)$ and $\Gamma_1 \mapsto \Gamma_1/(1 + \Delta)$ with $\Delta = A \exp[-(r/R - 1)^2/2\sigma^2]$. The size (or even the sign) of the surface term is essentially a property of the modelling methodology, and not physically meaningful; cf. Fig. 2 of Schmitt & Basu (2015). For this exercise we limit our attention to perturbations of a fixed relative size. In our subsequent discussion, we hold fixed the parameters of this perturbation (choosing $A = 0.2, \sigma = 0.002$), and examine its effects on three different stellar models at different points along a solar-calibrated evolutionary track, whose locations we show on a HR diagram in Fig. 2.

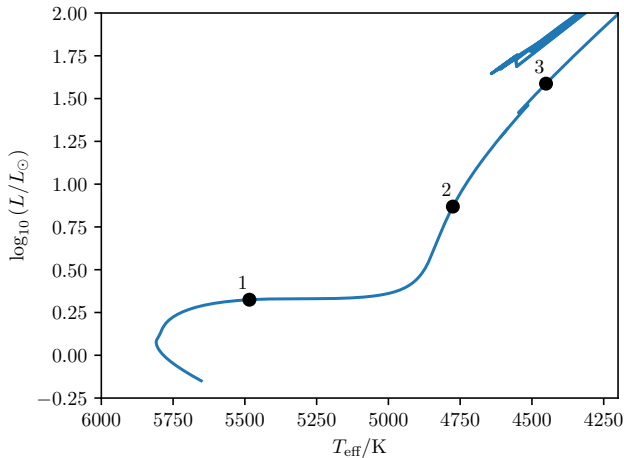


Figure 2. MESA evolutionary track with an initial mass of $1M_{\odot}$ and solar composition, with the stellar models in subsequent discussion numbered and marked out with black circles. We examine the effects of the simulated surface term on a young subgiant crossing the Hertzsprung gap, a young red giant near the base of the red giant branch, and an older red giant above the RGB bump.

Since we know a priori that the internal structures of our fiducial and perturbed models are identical, in principle the resulting cost functions should all be zero. Therefore, whatever values we do obtain serve as a relative diagnostic of the systematic error incurred by these approximations, or else-

where in the numerical method, relative to some estimate of the statistical error.

4.1. Subgiant

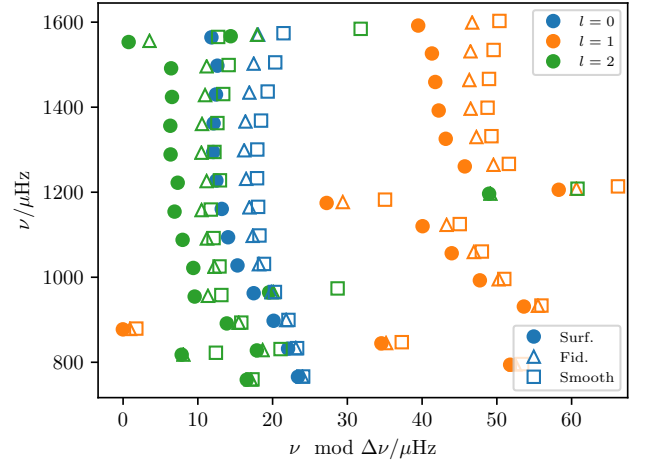


Figure 3. Frequency response of a young subgiant MESA model to a perturbation localised to the stellar surface. Mode frequencies from the fiducial model ($l = 0$) are shown with open upright triangles, and modes from a model with the surface perturbation applied ($l = 1$) are shown with filled circles. Additionally, modes from a slightly smoothed model (cf. later discussion in Section 4.1.2) are shown with open squares.

We first examine a young subgiant crossing the Hertzsprung gap (model 1 of Fig. 2). We compare the frequencies of the perturbed and fiducial model on an echelle diagram in Fig. 3. This particular model was chosen because its mode frequencies evince several instructive features:

- For the dipole modes, we see an on-resonance avoided crossing ($n_{\gamma} = 1$) near $\nu_{\max} \sim 1200 \mu\text{Hz}$, and a further off-resonance avoided crossing ($n_{\gamma} = 2$) at $\nu \sim 900 \mu\text{Hz}$. However, the π - γ coupling for dipole modes is strong enough for this off-resonance avoided crossing to produce significant frequency deviations from the asymptotic p -mode pattern, even several $\Delta\nu$ away from the underlying γ mode.
- For the quadrupole modes, we see one avoided crossing on resonance ($n_{\gamma} = 1$), two more avoided crossings slightly off resonance ($n_{\gamma} = 3$ and 4), and a g -dominated mode ($n_{\gamma} = 2$) near the dipole avoided crossing. The π - γ coupling is visibly much weaker for the quadrupole modes than the dipole modes.
- As we expect, the g -dominated modes are scarcely affected by the surface perturbation.

4.1.1. ϵ -matching

We now apply the ϵ -matching construction we derived in Section 3.1. For the sake of demonstration, we adopt a constant value of the mode frequency measurement error of $\sigma_{\nu} = 0.1 \mu\text{Hz}$, which is comparable to results returned from

Kepler (e.g. Li et al. 2020). In practice we should also expect these to increase away from ν_{\max} , as well as for g -dominated (and so lower-SNR) modes; we do not explicitly account for these other observational effects in this test. We show the resulting values of \mathcal{E}_l , and a fitted Chebyshev polynomial, in Fig. 4.

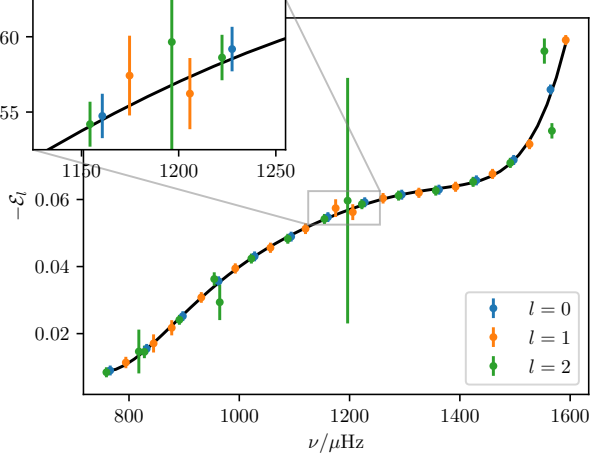


Figure 4. Results of applying the modified ϵ -matching procedure to the surface-perturbed subgiant model, shown in Fig. 3. We show computed values of \mathcal{E}_l with points, and a fitted Chebyshev polynomial with the black curve. Isolated avoided crossings result in a characteristic pattern of residuals that are first low, then high, on either side of the underlying resonant modes (as can be seen for dipole modes in inset panel).

We see in Fig. 4 that the p -dominated modes behave as we would expect: the residuals to a fit against a single l -independent function are dominated by mixed modes near the isolated avoided crossings. Moreover, we see from our definition in Eq. (33) that computing \mathcal{E}_l from g -dominated modes results in propagated measurement errors that are significantly inflated by their inertia ratios Q ; consequently they do not contribute substantially to the fit.

For our test case, we see that these systematic errors together lead to a reduced χ^2 statistic of $\chi_\epsilon^2 = 1.5$, where M is the order of the best-fitting Chebyshev polynomial. We interpret this as a diagnostic of the amount of systematic error incurred by our construction. Most of this can be attributed to the quadrupole modes near resonance, for which condition (II) appears not to hold (in particular for the $n_\gamma = 1$ avoided crossing at high frequencies) for this particular surface perturbation. This is in turn because the quadrupole coupling strength is of comparable size to the surface term perturbation, rendering a first-order construction insufficient; cf. the discussion in Fig. 1. Excluding these modes from the computation yields $\chi_\epsilon^2 = 0.13$, indicating that the first-order approximation works very well for the other modes. On the other hand, the coupling strength for dipole modes is an order of magnitude larger, and so the resulting systematic error in \mathcal{E}_1 is smaller than our adopted

trial measurement error, even near the on-resonance $n_\gamma = 1$ dipole avoided crossing (inset panel of Fig. 4).

Fig. 4 shows a characteristic pattern in the residuals of \mathcal{E}_l near each avoided crossing, where the values computed with Eq. (33) are first lower, then higher, than would be consistent with a single function of frequency. To leading order, this is the direct result of neglecting the overlap terms D_{ij} in Section 3.1. To see why this is so, let us consider the restricted example of a single π mode coupling to a single γ mode. This can be described as a perturbed eigenvalue problem of the form

$$\begin{bmatrix} -\omega_p^2 - \lambda V & \alpha - D\omega_\pi^2 \\ \alpha - D\omega_\pi^2 & -\omega_g^2 \end{bmatrix} \begin{bmatrix} c_p \\ c_g \end{bmatrix} = -\omega^2 \begin{bmatrix} 1 & D \\ D & 1 \end{bmatrix} \begin{bmatrix} c_p \\ c_g \end{bmatrix}, \quad (43)$$

with eigenvalues ω_\pm^2 , where D is the volume overlap integral defined in Eq. (2), and α is the π - γ coupling strength. Without loss of generality, we choose a normalisation of the eigenfunctions so that both are positive. Moreover, at an avoided crossing, the two modes are in resonance, so we set $\omega_p \sim \omega_g \sim \omega_\pi \sim \omega_0$. Here V represents the (small) frequency perturbation from the surface term, acting only on the p -mode subsystem, which is “turned on” as λ goes from 0 to 1.

Since this is a 2×2 problem, we can analytically evaluate the eigensystem of this eigenvalue problem at resonance. For the unperturbed problem ($\lambda \rightarrow 0$) we find that

$$\omega_\pm^2 = \omega_0^2 \pm \frac{\alpha}{1 \mp D}; \quad c_{g,\pm} = \mp c_p. \quad (44)$$

Let us first consider the result of neglecting D in our procedure. The frequency perturbations from the surface term can be found, to leading order, from perturbation theory with respect to this mixed mode basis using Eq. (7), as

$$\delta\omega_\pm^2 = \lambda V c_p (c_p + D c_{g,\pm}) + \mathcal{O}(\lambda^2) \sim \lambda c_p^2 (1 \mp D). \quad (45)$$

But our construction assumes $\delta\omega^2 \sim \lambda V c_p^2$ to first order — i.e. we have neglected the overlap terms in Eq. (31) — so per Eq. (33) we find that this causes us to systematically underestimate $\mathcal{E}_l(\nu_-)$ and overestimate $\mathcal{E}_l(\nu_+)$ for each isolated avoided crossing.

4.1.2. Sensitivity to interior differences

We now examine the ability of this procedure to discriminate between stars of differing interior structures. For this purpose, we again compute the eigensystems, of both mixed and π modes, of a model which is otherwise identical to the fiducial model, except for a very small amount of smoothing applied to the pressure and density gradients: 3 iterations of a box filter, 2 mesh points wide. We do this to ensure that the overall acoustic structure is only very slightly changed compared to the fiducial model.

We show the resulting mixed modes with open squares in Fig. 3. The effect of this smoothing on the p -modes is small and similar to that of a surface term: this can be seen from its effect on the radial modes. Unlike the surface term, this

smoothing also changes the avoided-crossing pattern, since the frequencies of the lowest-order γ modes are extremely sensitive to the Brunt-Väisälä frequency profile. In particular, the $n_\gamma = 1$ and $n_\gamma = 3$ quadrupole avoided crossings have now gone significantly off resonance.

Applying our ϵ -matching procedure to this smoothed model, we find that the changes to the underlying γ -modes lead to values of \mathcal{E}_l that are very large (Fig. 5), since they are heavily upweighted by the inertia ratios Q . These shifts cannot, and should not, be explicable by any surface term correction. Moreover, we find that the residuals of the mixed modes near the on-resonance avoided crossings no longer exhibit the characteristic jagged morphology we described in the preceding section. Even excluding the most g -dominated modes from the cost function of this procedure, by including only modes with $Q < 2$ in the cost function, we still obtain a reduced χ^2 of more than 200. We conclude that this technique is indeed able to diagnose even minor differences in interior structures.

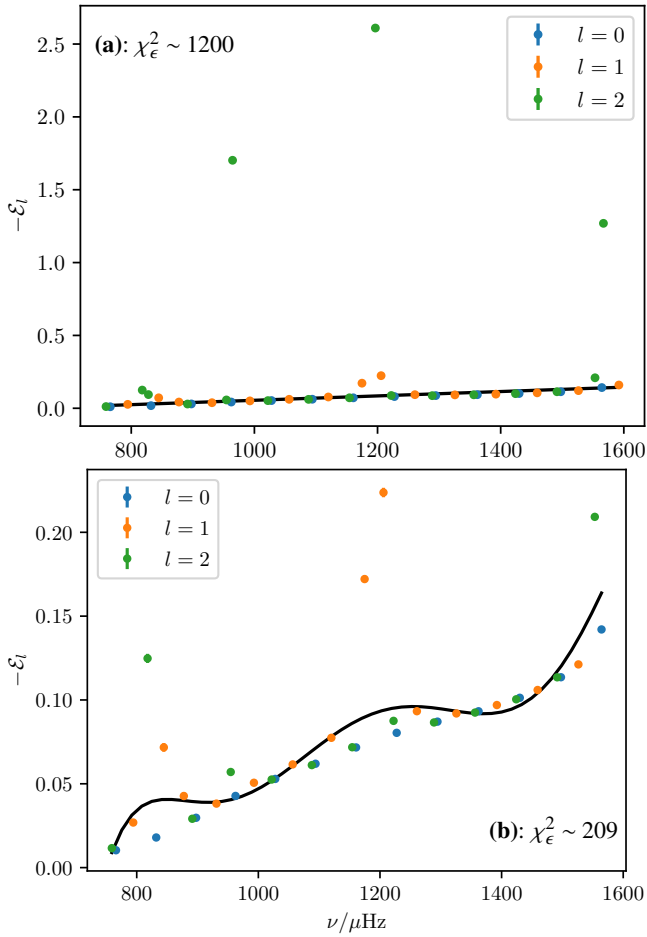


Figure 5. Results of applying the modified ϵ -matching procedure to a slightly smoothed model. Values of \mathcal{E}_l and a fitted Chebyshev polynomial are shown with the procedure applied to all modes in (a), and with the set of modes limited to those with $Q < 2$ in (b).

4.2. Young red giant

We next apply the same methodology to a slightly more evolved star (model 2 of Fig. 2). For this test we have used a young red giant (near the base of the red giant branch, but before the RGB bump) with $\Delta\nu = 17.5 \mu\text{Hz}$. We show its mode frequencies, as well as those of a model with the surface perturbation applied, in Fig. 6a. Of particular note here are a dipole avoided crossing at $\sim 290 \mu\text{Hz}$, and a quadrupole avoided crossing at $\sim 240 \mu\text{Hz}$, in the mode frequencies of the fiducial model.

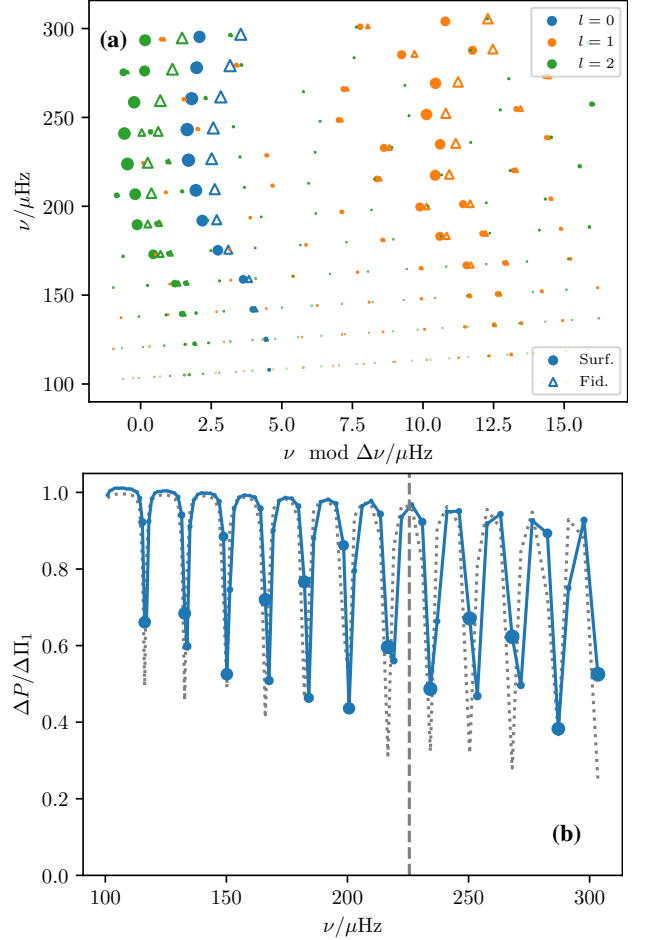


Figure 6. (a): Fiducial and perturbed frequencies of a young red giant model responding to a perturbation localised to the stellar surface. Markers and colours have the same meaning as in Fig. 3. Points are sized by mode inertia to indicate whether the modes shown are p- or g-dominated. (b): Local period differences between adjacent dipole modes as a function of frequency, showing ν_{\max} with the vertical dashed line. We show the g -mode inertia ratio $\zeta \sim 1 - c_\pi^2$ with the grey dotted line in the background.

Whereas the mixed modes for the subgiant shown in Fig. 3 feature the coupling of many π -modes to few γ -modes, the mixed modes in this case are the result of the opposite scenario (few π -modes to many γ -modes). From Fig. 1, we see

that this model lies close to the limits of validity of first-order perturbative constructions where the surface term is small (e.g. $\delta\nu_{\text{surf}} \sim 0.1\Delta\nu$) for quadrupole modes, and outside the formal radius of convergence for dipole modes. We also show in Fig. 6b the absolute first differences of the oscillation periods of the dipole modes, normalised by the asymptotic period spacing $\Delta\Pi_1$. When the g-modes are much denser than the p-modes, this quantity known to approximate the quantity $\zeta \sim 1 - c_\pi^2$, which takes values close to 1, except near the p-modes. We show ζ with the grey dotted line in the background. However, we can see that (particularly above ν_{max}) the g-modes are sparse enough that this is a poor approximation. Thus, this red giant is not yet so evolved that we may ignore mode mixing altogether, and rely solely on π -mode computations. In general, since the size of the surface-term perturbation increases with frequency, we will expect our approximations to work less well at higher frequencies than at lower frequencies.

We first apply our first-order construction from Section 3.1, limiting ourselves to only including modes where $Q < 5$. Again we assume a constant frequency uncertainty of $0.1 \mu\text{Hz}$. We show the resulting values of \mathcal{E}_l and the corresponding best-fitting Chebyshev polynomial in Fig. 7.

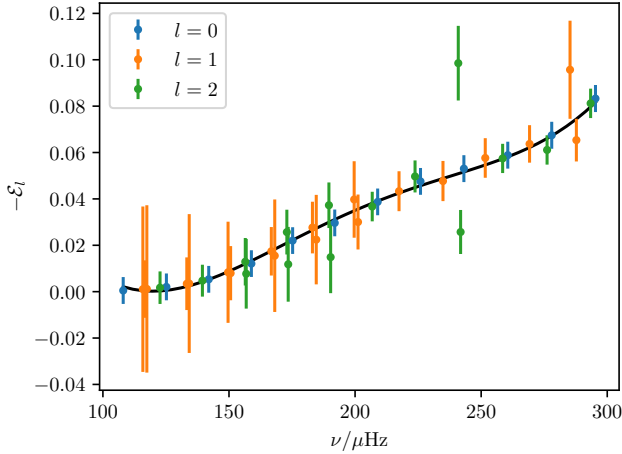


Figure 7. Result of applying our first-order construction to the perturbed model shown in Fig. 6. Symbols and lines have the same meanings as in Fig. 4.

The first-order procedure yields a reduced χ^2 statistic of $\chi_\epsilon^2 = 0.55$. As in Section 4.1, most of the deviation from a single function $\mathcal{F}(\nu)$ arises in the neighbourhood of avoided crossings, where the same jagged morphology emerges for the residuals, although the deviations are more pronounced here than previously. This is to be expected given the overall weaker coupling. In particular, we can see in Fig. 6 that the surface term is large enough, relative to the coupling strength, that the π mode participating in the quadrupole avoided crossing in the fiducial frequencies at $\sim 240 \mu\text{Hz}$ has been moved off resonance with the underlying γ mode. Once again, excluding this highest-frequency avoided quadrupole avoided

crossing from consideration yields a significantly reduced amount of systematic error, with $\chi_\epsilon^2 = 0.16$.

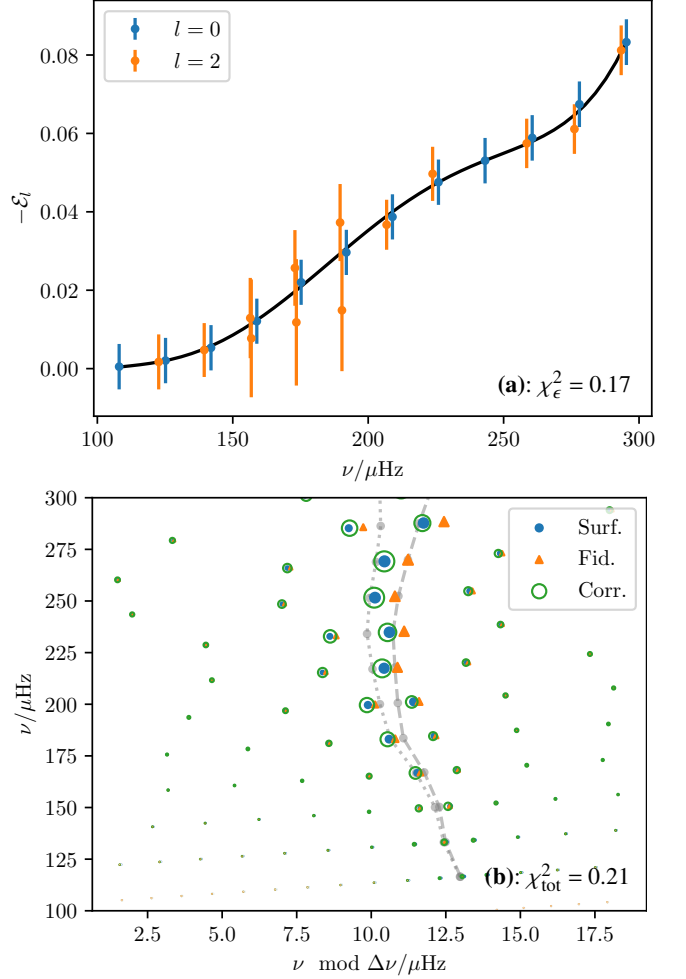


Figure 8. Illustration of the procedure described in Section 3.3, as applied to our young red giant model. (a) Modified ϵ -matching construction applied to only radial and quadrupole modes. (b) Dipole modes from both the surface-perturbed model (blue circles) and from the fiducial model, both without (orange triangles) and with (green open circles) the application of the surface correction implied by Eq. (39). Points are sized by the inverse mode inertia. We also show the underlying π -mode frequencies without (dashed grey line) and with (dotted grey line) this same correction.

For comparison, we also apply the generalised correction described in Section 3.3, fully accounting for the coupling between π and γ modes, which we illustrate in Fig. 8. In Fig. 8a, we show the results of applying the same modified ϵ -matching procedure, but restricted to only radial and quadrupole modes. This yields a best-fitting function $\mathcal{F}(\nu)$, which we used to generate corrected π -mode frequencies from those of the fiducial model via Eq. (39). These are then used to generate a full set of mixed modes by way of the prescription in Section 3.3,

which we show in Fig. 8b. In addition to mixed-mode frequencies, we also show the underlying π -modes of the fiducial model with and without the same correction being applied. The overall cost function from the combined procedure is $\chi_{\text{tot}}^2 = 0.21$.

From Fig. 8b, it is apparent that even where mixed modes in the fiducial model lie close to their underlying π modes, the corresponding corrected mixed mode frequencies may not necessarily lie close to the corrected π mode frequencies. This is unlike the behaviour of inertia-weighted corrections, which do not explicitly account for the locations of nearby γ modes. The matrix construction appears to do an adequate job of the correction, with a reduced cost function of $\chi_{\text{matrix}}^2 / (N_{\text{tot}} - N_{\epsilon} - 1) = 0.29$ (limiting ourselves again to only modes with $Q < 5$).

4.3. Evolved red giant

Finally, we consider these same methods as applied to a still more evolved red giant ($\Delta\nu = 3.9 \mu\text{Hz}$; model 3 of Fig. 2), with the same surface perturbation applied. We show the echelle diagram of its mode frequencies in Fig. 9a.

Generally speaking, the frequency measurement errors of these evolved stars are smaller than for subgiants (partly owing to the longer mode lifetimes). Consequently, for this exercise we adopt a measurement error of $0.025 \mu\text{Hz}$. This time, the size of the surface term perturbation is comparable to the local g -mode spacing. Accordingly, following our discussion in Section 2.3, we may opt to rely entirely on the π -mode system of our fiducial model, and eschew the computation of mixed modes altogether.

There are several ways this may be done. For one, we might note that the most p -dominated mixed mode frequencies from the model are essentially specified by the π modes. Where the coupling is weak, it is common practice (as done in e.g. Ball et al. 2018; McKeever et al. 2019; Chaplin et al. 2020; Ong et al. 2021, for quadrupole mixed modes) to simply match these up with the most p -dominated mixed modes in the observed set. For the dipole modes, we see from Fig. 9b that the g -modes are now sufficiently dense to also permit this approach. We compare the results of doing this against directly using the π -modes associated with the model instead (in both cases matching them up with the most p -dominated of the observed mixed modes) in Fig. 10a and b. Generally speaking, we see that the use of the model π modes yields clearly superior results, even for the dipole modes (where the coupling is less weak). This is because the dipole coupling strength is comparable to the local g -mode spacing. Consequently it is large enough that even the most p -dominated mixed mode, i.e. the one nearest to the corresponding π mode, contains contributions from multiple g -modes, and hence $Q > 1$, which inflates the estimate of \mathcal{E}_1 returned from Eq. (33). This is avoided by using the π modes directly.

On the other hand, restricting ourselves to only the most p -dominated modes means that we discard information from the nearby, more g -like mixed modes, which yield better constraints of the interior structure of the star. In order to include

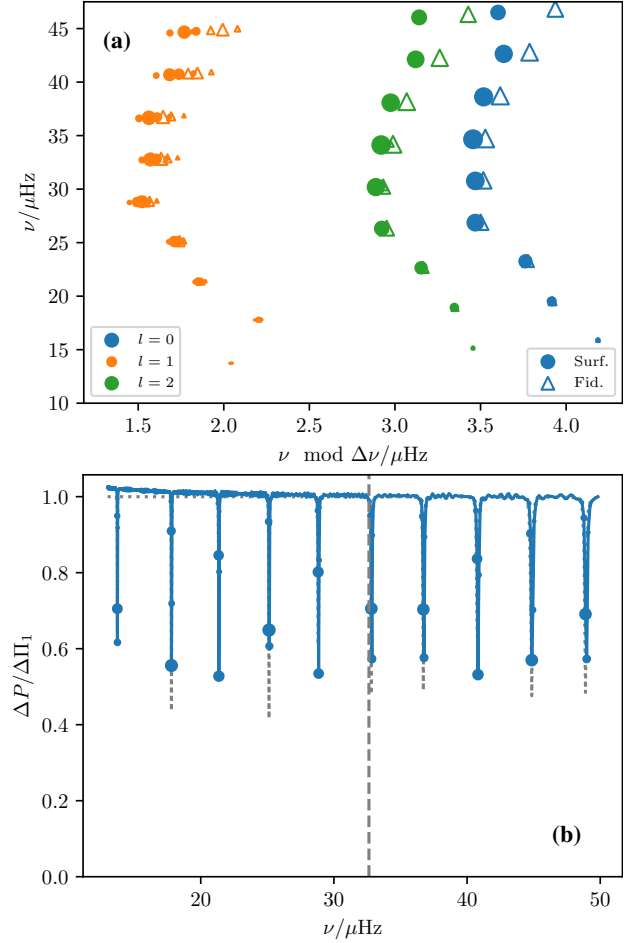


Figure 9. (a): Fiducial and perturbed frequencies of a evolved red giant model responding to a perturbation localised to the stellar surface. Markers and colours have the same meaning as in Figs. 3 and 6. We show only modes with $Q < 25$. Points are sized by mode inertiae to indicate whether the modes shown are p - or g -dominated. (b): Local period differences between adjacent dipole modes as a function of frequency, showing ν_{max} with the vertical dashed line. Again, we show the quantity $\zeta \sim 1 - c_{\pi}^2$ with the grey dotted line in the background.

these modes, we once again turn to the explicit matrix construction. As pointed out in Ball et al. (2018), only the very most p -dominated mixed modes are observationally accessible at quadrupole or higher degree, and for these modes the coupling strengths are so weak that the differences between their frequencies and those of the pure π modes is trivial, as can be seen in Fig. 10c. Accordingly, in this regime we may rely on these modes (in addition to the radial modes) to calibrate $\mathcal{F}(\nu)$ for use in correcting the dipole modes, and again feed this into Eq. (1) via the prescription of Section 3.3. We show the results of doing this in Fig. 10d. While the systematic error incurred by this approximation is still smaller than neglecting mode coupling altogether, we find that for this evolved red-giant regime the fundamental source of systematic error is instead the computation of the γ -mode matrix

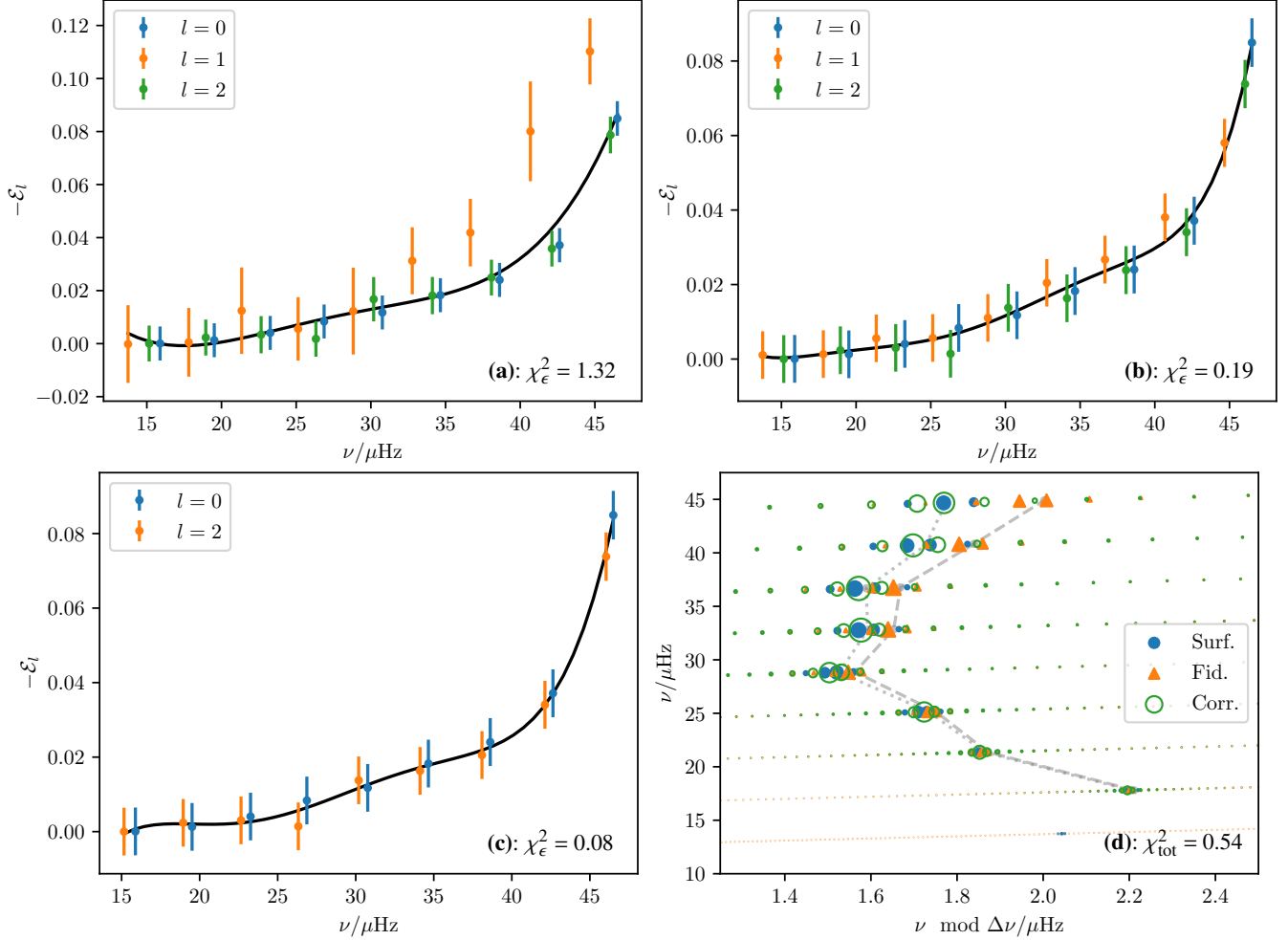


Figure 10. Application of different procedures to the perturbed model of Fig. 9. (a): ε -matching using the most p -dominated mixed modes in both the perturbed and fiducial frequency sets. (b): ε -matching of the most p -dominated mixed modes of the perturbed frequencies, matched with the fiducial π modes. (c): ε -matching procedure restricted to radial and p -dominated quadrupole modes, matched with the corresponding model π modes, in order to constrain $\mathcal{F}(\nu)$ independently of the dipole modes. (d): Dipole mixed modes computed via the prescription of Section 3.3 after applying the correction implied by $\mathcal{F}(\nu)$ as shown in panel (c).

elements, owing to underlying issues in the usual numerical scheme (see discussion in Appendix A).

Numerical issues aside, both the evaluation of these matrices, and solving their associated GHEPs, also become extremely expensive in this regime. Generally speaking, the coupling strength between any given pair of π and γ modes increases with the frequency of the γ mode, since the γ mode eigenfunctions become less oscillatory with frequency. Accordingly, for such evolved stars, the matrix elements of a very large number of γ modes has to be computed, including γ modes of much higher frequency than typically observed, so that the approximate coupling matrices which we actually use are sufficiently complete. Moreover, for a pair of $N \times N$ matrices, the solution of the corresponding GHEP has a runtime complexity of $O(N^3)$. For this single stellar model, the computation of these matrix elements took about 4 CPU hours on an Intel Xeon E5-2670 CPU running at 2.60 GHz. Thus, even if the numerical issues underlying the computation of the γ -mode

matrix elements are resolved, this procedure appears computationally impractical to apply at scale for the moment, at least for these evolved red giants.

4.3.1. Comparison with first-order approximation

In the solar case it is known that, in the absence of mode coupling, the surface term is well-approximated by a description of the form

$$\delta v_{\text{surf},nl} \sim f(\nu_{nl})/I_{nl}. \quad (46)$$

If they account for mode coupling at all, existing descriptions of the surface term treat mode coupling in precisely this manner (e.g. Kjeldsen et al. 2008; Ball & Gizon 2014; Pérez Hernández et al. 2016). In the absence of an a priori constraint on the size of the surface term, the function $f(\nu)$ is typically constrained (similarly to Section 3.3) with reference to only the radial modes, or a combination of the radial modes and most π -dominated quadrupole modes. We showed in Section 2.2 that using this expression directly to describe

the action of the surface term on the mixed modes, instead of performing the full matrix computation per Section 3.3, amounts to truncating the corresponding perturbative series expansion in powers of λ to first order in λ .

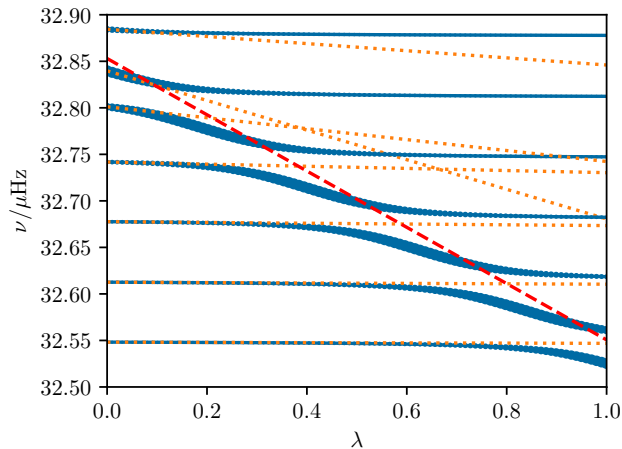


Figure 11. Interactions between mode mixing and the surface term, compared with the first-order approximation to mode coupling. The blue circles and lines show the frequencies of mixed modes obtained with different strengths of the surface term (parameterised by λ), while the orange dotted lines show the predicted mixed-mode frequencies upon application of an inertia-weighted correction of the form of Eq. (46). The red dashed line shows the evolution of the π -mode near these mixed modes, for which Eq. (46) is a much better approximation.

In Section 2.3, we derived that this perturbative series fails to converge when the surface term is larger than both the coupling strength and the local g-mode separation, which is the case for these evolved red giants. To illustrate the manner in which this approximation breaks down, we show in Fig. 11 the effects of applying an exaggeratedly large synthetic surface perturbation, with parameters $A = 1, \sigma = 0.002$, on the red giant model of the preceding section.

As before, we quantify the strength of the surface term with an interpolating parameter λ going from 0 to 1. The mixed-mode frequencies for a corresponding family of interpolated models are shown with filled blue circles (with sizes given as $1/Q$), overlaid on the solid blue curves. We also show the predicted frequency perturbations from applying a first-order correction, of the form Eq. (46), with the orange dotted lines. As expected from being first-order corrections, these take the form of straight lines, which are tangent to the blue curves at $\lambda = 0$. These first-order constructions may potentially change the ordering of the modes before and after their application (as noted in Ball et al. 2018; Li et al. 2018). We can see here that this is a fundamental limitation of first-order corrections in general, since the corresponding tangent lines may cross freely. Moreover, it is clear that when the surface term is large enough to change the ordering of the first-order predictions,

these predicted frequencies are entirely unreliable, even for the most p-dominated modes.

By contrast, the actual mixed modes undergo a series of avoided crossings, tracing out the trajectory of the underlying π -mode (shown with the red dashed line), which itself evolves in a linear fashion as the surface perturbation is “turned on”. Outside of the formal radius of convergence (Section 2.3), these avoided crossings defy linearisation (or, for that matter, approximation by power series), and are poorly approximated by their tangent lines at $\lambda = 0$. While the first-order construction still remains applicable to the bare π -modes, a full account of mode mixing is in principle mandatory for describing mixed modes in these situations.

At the same time, we have shown in the preceding section that for these evolved red giants, our existing implementation of the matrix machinery required for this is at once increasingly susceptible to numerical error, and prohibitively expensive to actually use. At present, it appears that we have little choice but to restrict our attention to the pure π -mode system when dealing with such red giants. While earlier works have raised concerns about potentially incurring systematic errors when doing so for dipole modes in particular (Ball et al. 2018; Ong et al. 2021), we have demonstrated in the preceding section that these are at least smaller than the typical statistical errors, and far preferable to the naive approach of using p-dominated mixed modes.

5. DISCUSSION AND CONCLUSION

The asteroseismic surface term arises as a consequence of structural differences between stellar models and actual stars, which in turn originate from modelling error localised to the near-surface layers. We have shown that the use of classical variational analysis for deriving frequency responses to these structural perturbations is implicitly equivalent to truncating a perturbative series expansion of the underlying eigenvalue problem to leading order in the perturbation operator.

This kind of first-order approximation holds good for pure p -modes, as well as for the π -mode subsystem of a star exhibiting mixed modes. However, such an approximation does not describe mixed modes well when the size of the frequency shift from the surface term is comparable to the coupling strength between the π and γ mode cavities. We have derived a more general matrix construction that remains valid in these cases. We have also derived both a first-order generalisation and an analogous matrix construction for the ϵ -matching algorithm described in Roxburgh (2016). From both analytic considerations (Section 2.3) and injection-recovery tests on stellar models (Section 4), we have shown that various sources of systematic error dominate for stellar models in different evolutionary stages. In particular we find that:

- Where the surface term is small compared to the coupling strength, existing methods may be used with minimal modification, so that mode coupling is accounted for to first order;

- Where the surface term is comparable to the coupling strength and/or the g-mode separation, such first-order analysis may not be adequate;
- Where the surface term is much larger than both the coupling strength and the g-mode separation, first-order constructions yield satisfactory results only when restricted to the π -mode subsystem. If mixed modes are to be explicitly considered at all, then in principle the full matrix computation of Section 3.3 must be used.
- For very evolved red giant stars, the full matrix construction becomes computationally impractical, and in any case we encounter an additional source of systematic error, arising from the numerical scheme used to compute γ -mode matrix elements at high order. In these cases, it appears for the time being that the only practical option is to limit attention to the behaviour of the π -mode subsystem.

One limitation of this analysis is that it is strictly applicable only to situations where both the fiducial and perturbed wave operator can be assumed to be Hermitian. By contrast, it is typically assumed that part of the surface term can be attributed to nonadiabatic wave propagation near the surface (typically neglected in pulsation calculations), which results in a non-Hermitian perturbation operator. Our analysis remains approximately applicable so long as the imaginary components of the nonadiabatic eigenvalues are small. However, in the more general, strongly nonadiabatic, case, a full non-Hermitian treatment (e.g. generalising the approach of Christensen-Dalsgaard 1981) may ultimately prove necessary.

The inferred values of certain global properties, such as stellar masses, radii, and ages, are known to be robust to different treatments of the surface term (Nsamba et al. 2018; Compton et al. 2018; Basu & Kinnane 2018) on the main sequence, where the observed modes are pure p-modes. They are, how-

ever, sensitive to these methodological choices (Jørgensen et al. 2020; Ong et al. 2021) for evolved red giants, where the observed modes are close to bare π -modes. Inferences of other properties, such as their initial helium abundances, have been shown to be sensitive to the choice of surface term treatment in both these extreme regimes, although the nature of this sensitivity exhibits qualitative differences. In Paper II, we examine the corresponding situation for subgiant stars, which lie in the intermediate regime.

These considerations are especially relevant given that, owing to observational limitations, the vast majority of known solar-like oscillators are evolved stars, and therefore exhibit mode mixing of some form. On the other hand, essentially all surface-term corrections in the literature (see e.g. Jørgensen et al. 2020, for a review) only account for mode mixing to first order, if at all. Given that almost all stars on the *TESS* short-cadence asteroseismic target list are subgiants, it is imperative that surface-term systematics of the kind we studied in Ong et al. (2021) be properly identified and characterised for subgiants in particular. The constructions we have presented in this work are essential to this task.

ACKNOWLEDGMENTS

We thank U. Banik, B. Mosser, and the anonymous referee for constructive feedback; we also thank R. Townsend for technical assistance with *GYRE*. We have made available Python scripts to evaluate the matrix elements discussed here and in OB20 at <https://gitlab.com/darthoctopus/mesa-tricks>. This work was partially supported by NASA K2 GO Award 80NSSC19K0102 and NASA TESS GO Award 80NSSC19K0374.

Software: NumPy (Harris et al. 2020), SciPy stack (Jones et al. 2001–), AstroPy (Astropy Collaboration et al. 2013; Price-Whelan et al. 2018), Pandas (McKinney 2010), MESA (Paxton et al. 2011, 2013, 2018), *GYRE* (Townsend & Teitler 2013).

APPENDIX

A. γ -MODE FREQUENCY CORRECTION

We recall that linear adiabatic oscillations in a nonrotating star can be expressed as linear combinations of displacement eigenfunctions

$$\vec{\xi}(r, \theta, \phi, t) = e^{\pm i\omega t} \left(\xi_r(r) \mathbf{Y}_l^m + \xi_h(r) \mathbf{\Psi}_l^m \right) \quad (\text{A1})$$

which emerge as solutions to the system of differential equations

$$\begin{aligned} \frac{1}{r^2} \frac{d}{dr} (r^2 \xi_r) - \frac{g}{c_s^2} \xi_r + \left(\alpha_\gamma - \frac{S_l^2}{\omega^2} \right) \frac{P_1}{\rho c_s^2} &= \frac{\Lambda^2}{\omega^2} \Phi_1, \\ \frac{1}{\rho} \frac{dP_1}{dr} + \frac{g}{c_s^2} P_1 + (\alpha_\pi N^2 - \omega^2) \xi_r &= -\frac{d\Phi_1}{dr}, \\ \frac{1}{r^2} \frac{d}{dr} \left(r^2 \frac{d\Phi_1}{dr} \right) - \frac{\Lambda^2}{r^2} \Phi_1 &= 4\pi G \rho \left(\frac{P_1}{\rho c_s^2} + \frac{N^2}{g} \xi_r \right) \\ \xi_h &= \frac{1}{r\omega^2} \left(\frac{P_1}{\rho} + \Phi_1 \right). \end{aligned} \quad (\text{A2})$$

We adopt the notational convention that all scalar perturbed quantities admit separation of variables as, e.g.,

$$\rho'(r, \theta, \phi) = \rho_{lmn}(r) Y_l^m(\theta, \phi). \quad (\text{A3})$$

Under ordinary circumstances, $\alpha_\gamma = \alpha_\pi = 1$. In Ong & Basu (2020), we demonstrated that isolation of the π and γ mode cavities can be effected by setting $\alpha_\pi = 0$ or $\alpha_\gamma = 0$, respectively. The full set of mixed-mode eigenvalues can then be recovered by solving the GHEP Eq. (1), where the matrix elements are specified by integrals taken with respect to the π and γ mode eigenfunctions.

The expression we derived for the coupling matrix elements within the $\gamma\gamma$ subspace in our previous paper assumes that the definition of the tangential component of the displacement wavefunction is modified. We showed previously that this results in a non-Hermitian wave operator. This is an undesirable property, and further investigation reveals it to yield results that are numerically inconsistent with mixed modes obtained from integrating the full equations. We now derive a Hermitian expression for this $\gamma\gamma$ coupling matrix, following from a different set of physical assumptions.

Specifically, we express the first line of Eq. (A2) in coordinate-free form by modifying the continuity equation, which we write as

$$\rho' + \nabla \cdot (\rho \vec{\xi}) = (1 - \alpha_\gamma) \frac{P'}{c_s^2}, \quad (\text{A4})$$

from which we can eliminate the density via the adiabatic relation

$$\rho' = \frac{P'}{c_s^2} + \rho \vec{\xi} \cdot \left(\frac{1}{\rho c_s^2} \nabla P - \frac{1}{\rho} \nabla \rho \right) \quad (\text{A5})$$

to obtain the desired result:

$$\nabla \cdot \vec{\xi} + \alpha_\gamma \frac{P'}{\rho c_s^2} + \frac{1}{\rho c_s^2} \vec{\xi} \cdot \nabla P = 0. \quad (\text{A6})$$

On the other hand, the time-independent wave operator acts on the momentum equation:

$$\mathcal{L} \vec{\xi} = -\omega^2 \rho \vec{\xi} = -\nabla P' + \rho' \vec{g} - \rho \nabla \Phi'. \quad (\text{A7})$$

As in our last paper, we define the γ -mode wave operator \mathcal{L}_γ to be the wave operator whose orthogonal basis functions are the eigenfunctions of the system of equations (Eq. (A2)) with $\alpha_\gamma \rightarrow 0$; it is related to the full time-independent wave operator as $\mathcal{L}_{\text{tot}} \equiv \mathcal{L}_\gamma + R_\gamma$. Under ordinary circumstances ($\alpha_\gamma = 1$), the right-hand-side of Eq. (A4) vanishes, allowing us to eliminate ρ' , P' , and Φ' from Eq. (A7) in favour of the displacement eigenfunctions, yielding the usual, manifestly Hermitian expression

$$\mathcal{L}_{\text{tot}} \vec{\xi} = \nabla \cdot \left(\vec{\xi} \cdot \nabla P + c_s^2 \rho \nabla \cdot \vec{\xi} \right) - \vec{g} \cdot (\rho \vec{\xi}) - \rho G \nabla \cdot \left(\int d^3 x' \frac{\nabla \cdot (\rho \vec{\xi}')}{|x - x'|} \right). \quad (\text{A8})$$

Comparing Eq. (A8) with Eq. (A6), we see that the first term of Eq. (A8) vanishes when the full wave operator acts on γ

modes (so that $\alpha_\gamma = 0$). Consequently, the action of the total wave operator on γ modes is such that

$$\mathcal{L}_{\text{tot}} \vec{\xi}_\gamma = -\vec{g} \cdot (\rho \vec{\xi}_\gamma) - \rho G \nabla \cdot \left(\int d^3 x' \frac{\nabla \cdot (\rho \vec{\xi}'_\gamma)}{|x - x'|} \right). \quad (\text{A9})$$

With the displacement wavefunctions normalised so that

$$\int d^3 x \rho \vec{\xi}_{\gamma,i} \cdot \vec{\xi}_{\gamma,j} = \delta_{ij} \quad (\text{A10})$$

where each of i, j stands in for the relevant multi-index n, l, m of the corresponding mode, we define the matrix $\mathbf{L}_{\gamma\gamma}$ with elements specified as

$$\begin{aligned} L_{\gamma\gamma,ij} &= \left\langle \vec{\xi}_{\gamma,i}, \mathcal{L} \vec{\xi}_{\gamma,j} \right\rangle \\ &= \int d^3 x \vec{\xi}_{\gamma,i} \cdot \left(-\vec{g} \cdot (\rho \vec{\xi}_{\gamma,j}) - \rho G \nabla \cdot \left(\int d^3 x' \frac{\nabla \cdot (\rho \vec{\xi}'_{\gamma,j})}{|x - x'|} \right) \right) \\ &\equiv -\omega_{\gamma,i}^2 \delta_{ij} + R_{\gamma\gamma,ij}. \end{aligned} \quad (\text{A11})$$

On the other hand, we may also perform this kind of elimination directly on the γ -mode wave operator subject to the modified continuity equation Eq. (A4). Since the right-hand-side no longer vanishes, we cannot eliminate the pressure directly. Instead, we obtain

$$\mathcal{L}_\gamma \vec{\xi}_\gamma = -\nabla P' + \vec{g} \cdot \left(\frac{P'}{c_s^2} - \nabla \cdot (\rho \vec{\xi}_\gamma) \right) + \rho G \nabla \cdot \left(\int d^3 x' \frac{\left(\frac{P'}{c_s^2} - \nabla \cdot (\rho \vec{\xi}'_\gamma) \right)}{|x - x'|} \right). \quad (\text{A12})$$

Under the action of the inner product, the first term can be integrated by parts, yielding a surface integral that vanishes, given that the displacement wavefunctions for γ -modes also vanish on the outer boundary. We then obtain

$$\int d^3 x \vec{\xi}_{\gamma,i} \cdot \left(-\nabla P'_j + \vec{g} \cdot \frac{P'_j}{c_s^2} \right) = \int d^3 x P'_j \cdot \left(\nabla \cdot \vec{\xi}_{\gamma,i} + \frac{1}{\rho c_s^2} \vec{\xi}_{\gamma,i} \cdot \nabla P \right) = 0, \quad (\text{A13})$$

by Eq. (A6). Therefore, within the γ -mode system, we have an explicit expression for $R_{\gamma\gamma,ij}$, which are the matrix elements of $\mathcal{R}_\gamma = \mathcal{L}_{\text{tot}} - \mathcal{L}_\gamma$:

$$R_{\gamma\gamma,ij} = -G \int d^3 x \rho \vec{\xi}_{\gamma,i} \cdot \nabla \cdot \left(\int d^3 x' \frac{P'_j / c_s^2}{|x - x'|} \right). \quad (\text{A14})$$

We have found these two expressions to be consistent with each other, and with Eq. (3) when used to evaluate $R_{\pi\gamma}$.

A.1. Systematic Errors

The primary source of error in this computation depends strongly on the order of the modes under consideration. It is well-known that numerical solutions of the boundary-value problem, under the usual boundary conditions typically used in asteroseismology, yield basis functions that are only approximately orthonormal when the domain of integration is

bounded. Generally speaking, this is because orthonormality of the eigenfunctions requires that certain surface integrals vanish when integrating by parts; however, in practice this is only true under certain restricted choices of boundary conditions, which are not typically used for seismic modelling. In deriving the above expressions we have made similar assumptions, and therefore incur errors of a similar kind. These systematic errors are small in a relative sense, and become most significant at low n_g . By contrast, at high n_g , the integrands become highly oscillatory, and potentially yield accumulated truncation error which increases with n_g . Again, this error is small in a relative sense.

On the other hand, we require low absolute — rather than relative — integration error, in order to accurately describe the γ -modes. In particular, given an asymptotic relation of the form

$$P_{l,n_g} \sim \Delta \Pi_l(n_g + \epsilon_{g,l}(n_g)), \quad (\text{A15})$$

we require that ϵ_g be estimated accurately in order to correctly describe the mixed-mode avoided crossings. To illustrate how both these sources of error scale with n_g , we estimate the relative error $\delta P_{n_g}/P_{n_g}$ by evaluating the inner product $\langle \vec{\xi}_{n_g}, \vec{\xi}_{n_g+1} \rangle$ for the γ -modes of the red giant model in Section 4.3; in the absence of both sources of error this should yield 0 everywhere. This is a relative error estimate because the mode eigenfunctions are all normalised to yield $\langle \vec{\xi}_{n_g}, \vec{\xi}_{n_g} \rangle = 1$. We find the corresponding absolute integration error in ϵ_g using Eq. (A15), showing the results in Fig. 12.

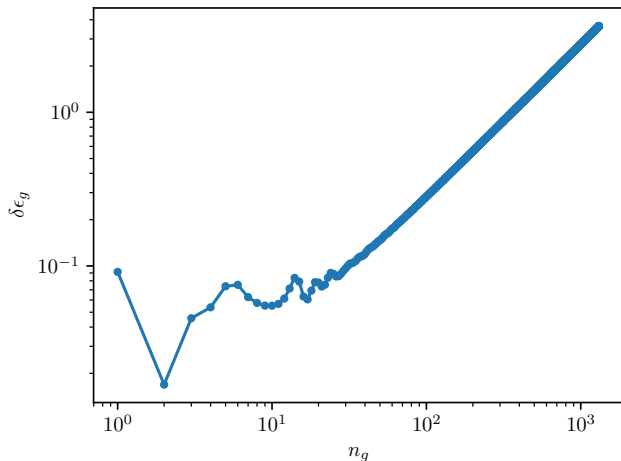


Figure 12. Estimate of the truncated absolute integration error in the g-mode phase function ϵ_g , as a function of the g-mode radial order n_g (see text for complete description).

We see that for $n_g \lesssim 100$, these integration errors are small. However, as n_g continues to increase, this absolute error appears to grow without bound. In our numerical implementation, we have fitted a slowly-varying correction to the diagonal elements of the γ -mode subsystem as a polynomial in the frequency, whose coefficients are chosen to minimise the sum of squared differences between g-dominated mixed-mode frequencies from this matrix construction, compared to those returned directly from GYRE. Even so, Fig. 12 indicates that this strategy is not tenable for $n_g \gtrsim 200$.

REFERENCES

- Aizenman, M., Smeyers, P., & Weigert, A. 1977, *A&A*, 58, 41
 Astropy Collaboration, Robitaille, T. P., Tollerud, E. J., et al. 2013, *A&A*, 558, A33, doi: [10.1051/0004-6361/201322068](https://doi.org/10.1051/0004-6361/201322068)
 Babikov, V. V. 1976, *A method of phase functions in Quantum mechanics* (Moscow: Nauka)
 Ball, W. H., & Gizon, L. 2014, *A&A*, 568, A123, doi: [10.1051/0004-6361/201424325](https://doi.org/10.1051/0004-6361/201424325)
 Ball, W. H., Themeßl, N., & Hekker, S. 2018, *MNRAS*, 478, 4697, doi: [10.1093/mnras/sty1141](https://doi.org/10.1093/mnras/sty1141)
 Basu, S., & Kinnane, A. 2018, *ApJ*, 869, 8, doi: [10.3847/1538-4357/aae922](https://doi.org/10.3847/1538-4357/aae922)

- Benomar, O., Bedding, T. R., Stello, D., et al. 2012, *ApJL*, 745, L33, doi: [10.1088/2041-8205/745/2/L33](https://doi.org/10.1088/2041-8205/745/2/L33)
- Calogero, F. 1963, *Il Nuovo Cimento*, 27, 261, doi: [10.1007/BF02812620](https://doi.org/10.1007/BF02812620)
- Chaplin, W. J., Serenelli, A. M., Miglio, A., et al. 2020, *Nature Astronomy*, 4, 382, doi: [10.1038/s41550-019-0975-9](https://doi.org/10.1038/s41550-019-0975-9)
- Christensen-Dalsgaard, J. 1981, *MNRAS*, 194, 229, doi: [10.1093/mnras/194.2.229](https://doi.org/10.1093/mnras/194.2.229)
- Compton, D. L., Bedding, T. R., Ball, W. H., et al. 2018, *MNRAS*, 479, 4416, doi: [10.1093/mnras/sty1632](https://doi.org/10.1093/mnras/sty1632)
- Gough, D. 1990, in *Progress of Seismology of the Sun and Stars*, ed. Y. Osaki & H. Shibahashi (Berlin, Heidelberg: Springer Berlin Heidelberg), 281–318, doi: [10.1007/3-540-53091-6](https://doi.org/10.1007/3-540-53091-6)
- Gough, D. O., & Thompson, M. J. 1990, *MNRAS*, 242, 25, doi: [10.1093/mnras/242.1.25](https://doi.org/10.1093/mnras/242.1.25)
- Grevesse, N., & Sauval, A. J. 1998, *SSRv*, 85, 161, doi: [10.1023/A:1005161325181](https://doi.org/10.1023/A:1005161325181)
- Harris, C. R., Millman, K. J., van der Walt, S. J., et al. 2020, *Nature*, 585, 357
- Jones, E., Oliphant, T., Peterson, P., et al. 2001–, *SciPy: Open source scientific tools for Python*. <http://www.scipy.org/>
- Jørgensen, A. C. S., Montalbán, J., Miglio, A., et al. 2020, *MNRAS*, 495, 4965, doi: [10.1093/mnras/staa1480](https://doi.org/10.1093/mnras/staa1480)
- Kjeldsen, H., Bedding, T. R., & Christensen-Dalsgaard, J. 2008, *ApJL*, 683, L175, doi: [10.1086/591667](https://doi.org/10.1086/591667)
- Li, T., Bedding, T. R., Huber, D., et al. 2018, *MNRAS*, 475, 981, doi: [10.1093/mnras/stx3079](https://doi.org/10.1093/mnras/stx3079)
- Li, Y., Bedding, T. R., Li, T., et al. 2020, *MNRAS*, 495, 2363, doi: [10.1093/mnras/staa1335](https://doi.org/10.1093/mnras/staa1335)
- Lynden-Bell, D., & Ostriker, J. P. 1967, *MNRAS*, 136, 293, doi: [10.1093/mnras/136.3.293](https://doi.org/10.1093/mnras/136.3.293)
- McKeever, J. M., Basu, S., & Corsaro, E. 2019, *ApJ*, 874, 180, doi: [10.3847/1538-4357/ab0c04](https://doi.org/10.3847/1538-4357/ab0c04)
- McKinney, W. 2010, in *Proceedings of the 9th Python in Science Conference*, ed. S. van der Walt & J. Millman, 51 – 56
- Nsamba, B., Campante, T. L., Monteiro, M. J. P. F. G., et al. 2018, *MNRAS*, 477, 5052, doi: [10.1093/mnras/sty948](https://doi.org/10.1093/mnras/sty948)
- Ong, J. M. J., & Basu, S. 2019, *ApJ*, 885, 26, doi: [10.3847/1538-4357/ab425f](https://doi.org/10.3847/1538-4357/ab425f)
- . 2020, *ApJ*, 898, 127, doi: [10.3847/1538-4357/ab9ffb](https://doi.org/10.3847/1538-4357/ab9ffb)
- Ong, J. M. J., Basu, S., & McKeever, J. M. 2021, *ApJ*, 906, 54, doi: [10.3847/1538-4357/abc7c1](https://doi.org/10.3847/1538-4357/abc7c1)
- Ong, J. M. J., Lund, M., Bieryla, A., et al. submitted to *ApJ*
- Otí Floranes, H., Christensen-Dalsgaard, J., & Thompson, M. J. 2005, *MNRAS*, 356, 671, doi: [10.1111/j.1365-2966.2004.08487.x](https://doi.org/10.1111/j.1365-2966.2004.08487.x)
- Paxton, B., Bildsten, L., Dotter, A., et al. 2011, *ApJS*, 192, 3, doi: [10.1088/0067-0049/192/1/3](https://doi.org/10.1088/0067-0049/192/1/3)
- Paxton, B., Cantiello, M., Arras, P., et al. 2013, *ApJS*, 208, 4, doi: [10.1088/0067-0049/208/1/4](https://doi.org/10.1088/0067-0049/208/1/4)
- Paxton, B., Schwab, J., Bauer, E. B., et al. 2018, *ApJS*, 234, 34, doi: [10.3847/1538-4365/aaa5a8](https://doi.org/10.3847/1538-4365/aaa5a8)
- Pérez Hernández, F., García, R. A., Corsaro, E., Triana, S. A., & De Ridder, J. 2016, *A&A*, 591, A99, doi: [10.1051/0004-6361/201628311](https://doi.org/10.1051/0004-6361/201628311)
- Pontin, C. M., Barker, A. J., Hollerbach, R., André, Q., & Mathis, S. 2020, *MNRAS*, 493, 5788, doi: [10.1093/mnras/staa664](https://doi.org/10.1093/mnras/staa664)
- Price-Whelan, A. M., Sipőcz, B. M., Günther, H. M., et al. 2018, *AJ*, 156, 123, doi: [10.3847/1538-3881/aabc4f](https://doi.org/10.3847/1538-3881/aabc4f)
- Roxburgh, I. W. 2005, *A&A*, 434, 665, doi: [10.1051/0004-6361:20041957](https://doi.org/10.1051/0004-6361:20041957)
- . 2015, *A&A*, 574, A45, doi: [10.1051/0004-6361/201425289](https://doi.org/10.1051/0004-6361/201425289)
- . 2016, *A&A*, 585, A63, doi: [10.1051/0004-6361/201526593](https://doi.org/10.1051/0004-6361/201526593)
- Roxburgh, I. W., & Vorontsov, S. V. 2003, *A&A*, 411, 215, doi: [10.1051/0004-6361:20031318](https://doi.org/10.1051/0004-6361:20031318)
- Schmitt, J. R., & Basu, S. 2015, *ApJ*, 808, 123, doi: [10.1088/0004-637X/808/2/123](https://doi.org/10.1088/0004-637X/808/2/123)
- Sonoi, T., Samadi, R., Belkacem, K., et al. 2015, *A&A*, 583, A112, doi: [10.1051/0004-6361/201526838](https://doi.org/10.1051/0004-6361/201526838)
- Townsend, R. H. D., & Teitler, S. A. 2013, *MNRAS*, 435, 3406, doi: [10.1093/mnras/stt1533](https://doi.org/10.1093/mnras/stt1533)